"In presenting the dissertation as a partial fulfillment of the requirements for an advanced degree from the Georgia Institute of Technology, I agree that the Library of the Institution shall make it available for inspection and circulation in accordance with its regulations governing materials of this type. I agree that permission to copy from, or to publish from, this dissertation may be granted by the professor under whose direction it was written, or such copying or publication is solely for scholarly purposes and does not involve potential financial gain. It is understood that any copying from, or publication of, this dissertation which involves potential financial gain will not be allowed without written permission.

_____

"

12T

AN INVESTIGATION OF FRICTION COEFFICIENTS IN THE INLET LENGTH OF SMOOTH ROUND TUBES

A THESIS

Presented to

the Faculty of the Graduate Division

by

William Elijah Huie

In Partial Fulfillment

of the Requirements for the Degree

Master of Science in Mechanical Engineering

Georgia Institute of Technology

September 1953

AN INVESTIGATION OF FRICTION COEFFICIENTS

IN THE INLET LENGTH OF SMOOTH ROUND TUBES

Approved:

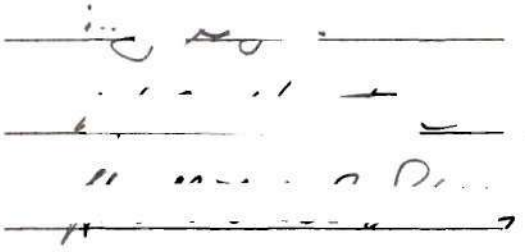

Date Approved by Chairman: 1 September 1953

TABLE OF CONTENTS

LIST OF TABLES

(Continued)

LIST OF TABLES (Continued)

LIST OF ILLUSTRATIONS

(Continued)

*Figures 1 through 22 refer to graphs of ratios of local and integrated apparent friction coefficients to the Karman-Nikuradse friction coefficient versus L/D ratios for the test indicated.

LIST OF ILLUSTRATIONS (Continued)

SYMBOLS

D	tube diameter, feet
ΔP	pressure drop between taps, inches of water
f_{APP}	apparent friction coefficient, dimensionless
$\overline{f}_{APP}$	integrated apparent friction coefficient, dimensionless
f_{K-N}	Karman-Nikuradse coefficient, dimensionless
L/D	ratio of distance from inlet to tube diameter
P	static pressure, feet of water
P_{cc}	pressure in calming chamber, psig
psig	pounds per square inch gage pressure
R_D	Reynolds number based on tube diameter, dimensionless
R_X	Reynolds number based on distance from tube inlet, dimensionless
T_w	temperature of water flowing through apparatus, °F.
W_w	weight of water flowing through apparatus, pounds per minute
V	mean velocity based on mass rate of flow, feet per second
X	distance from tube inlet, feet
	viscosity, slugs per foot-second
	density, slugs per cubic foot

SUMMARY

An experimental investigation was made of apparent friction coefficients in the inlet length of smooth, round tubes with bellmouth entrances. Tests were conducted with flow of water through one-half inch, three-quarter inch and one inch copper tubing at Reynolds numbers varying from 46,000 to 333,000.

The results were recorded in terms of the local apparent friction coefficient and the integrated apparent friction coefficient. The apparent friction coefficient is a direct measure of the pressure loss and includes the effects of both friction and momentum flux changes. The integrated value of the coefficient is simply a measure of the total loss from the tube inlet to the point concerned.

The tests indicated that an undetermined amount of turbulence existed at the tube inlet. This induced turbulence greatly affected the boundary layer and the friction coefficients within the inlet length. The results indicated that, for flow through the one-half inch tube and for flow at Reynolds numbers less than 125,000 through the one inch tube, the boundary layer was initially laminar with a transition to turbulent boundary layer at an average Reynolds number (based on distance from the tube inlet) of about 500,000. This value compared well with the corresponding value for a flat plate. For flow through the three-quarter inch tube and

for flow at Reynolds numbers greater than 125,000 through the one inch tube, it was found that the initial turbulence caused the boundary layer to be turbulent from the beginning of the observed inlet length.

Within the inlet length, the local apparent friction coefficient was found to vary widely from the Karman-Nikuradse coefficient for fully developed turbulent flow. The variations of the coefficient consisted of an initial decrease within the region of laminar boundary layer, an increase accompanying the transition to turbulent boundary layer, a second sharp decrease and subsequent fluctuations due to adjustments in velocity profile. However, the initial decrease and increase were absent in the tests for which no laminar boundary layer existed. Initial turbulence induced by the entrance greatly increased the magnitude of the variations in the values of friction coefficients in the zone of turbulent boundary layer. Also, elimination of the laminar boundary layer by induced turbulence acted to greatly increase the value of the friction coefficient in the region which would normally be the laminar inlet zone.

The experimental results tended to be in general agreement with the results of a similar investigation conducted by Shapiro and Smith and published in N.A.C.A. Technical Note #1785.

CHAPTER I

INTRODUCTION

Object.--The object of this investigation was to determine experimentally the values of apparent friction coefficients in the inlet length of round, smooth tubes and to find the effect on the friction coefficient of Reynolds number and distance from the entrance. It was anticipated that the results of the tests, conducted with the flow of water at Reynolds numbers corresponding to fully developed turbulent flow, would verify and supplement the results obtained by Shapiro and Smith in a similar investigation completed in 1947 and published in N.A.C.A. Technical Note #1785.

Survey of literature.--When a fluid from a calm source flows steadily through a horizontal tube of uniform diameter, the velocity profile in the region immediately downstream from the entrance varies with distance from the entrance. After this distance has become sufficiently great, the variations in the flow pattern disappear and the velocity profile remains unchanged. This length, wherein the flow pattern is developing, is referred to as the "length of transition" or the "inlet length."

The changes in velocity profile in the inlet length have an important effect upon the friction coefficient in this region. It has been found that the friction coefficient varies appreciably within the initial portion of the inlet length. At the end of the inlet region, the friction coefficient approaches a constant value and becomes independent of the distance from the tube inlet. However, even though values of friction

coefficients for the fully developed region have been accurately established, only scant and inconclusive data are available for the inlet length.

The usual procedure for calculating friction coefficients from pressure-loss data is to assume that the velocity profile is constant at each cross section. However, within the inlet length, this procedure does not consider the momentum flux changes accompanying the changes in velocity profile, and, therefore, the resulting friction coefficient does not represent the true drag coefficient. Friction coefficients calculated in this manner are designated "apparent friction coefficients." The "true friction coefficient" or the ratio of the wall shearing stress to the velocity head is equal to the "apparent friction coefficient" only when the velocity profile is constant at all cross sections and the flow is incompressible. Therefore, in order to calculate values of true friction coefficients within the inlet length, the changes in velocity profile must be determined.

With varying results, a certain amount of analytical work has been done in connection with velocity profiles and pressure losses within the length of transition.

Boussinesq (1), in 1890, obtained a solution for the development of the velocity profile for laminar flow. From his results, it was concluded that for purely laminar flow, the length of transition in terms of a length-diameter ratio was

$$L/D = 0.065\ R_D.$$

Schiller (2), in an investigation of laminar flow, assumed that the typical velocity profile near the inlet was composed of a straight

line segment terminated by parabolic arcs. He then applied Karman's momentum equation to the entire cross section and the Bernoulli equation to the central core of fluid. The rate of development of the velocity profile was computed and the pressure drop from the inlet predicted. For the length of transition, Schiller obtained the ratio

$$L/D = 0.029\ R_D.$$

Langhaar (3) completed an analysis for laminar flow by employing a linearizing technique with the Navier-Stokes equation and retaining more terms than previous investigators. He assumed that the velocity was constant over the entire inlet cross section. Tests by Nikuradse justified this approximation for tubes with short bell-mouthed entries. Velocity profiles and pressure losses may be computed from Langhaar's results. The velocity profile was found to approach the fully developed parabolic form in asymptotic fashion. The length required for the center-line velocity to reach 99 per cent of its ultimate value was predicted to be

$$L/D = 0.058\ R_D.$$

The development of the velocity profile for turbulent flow was analyzed by Latzko (4). After assuming that a typical profile was composed of a straight-line segment terminated by arcs, Latzko obtained for the length of a purely turbulent inlet length the ratio

$$L/D = 0.69\ R_D^{0.25}.$$

Experimental investigations of the inlet length for turbulent flow seem to be few in number, limited in scope, and inconclusive in results.

Kirsten (5) measured velocity profiles at various distances from bellmouth entrances for the flow of air through smooth tubes. His results indicated that the boundary layer near the entrance was initially laminar with a subsequent change to the type of combined laminar and turbulent boundary layer associated with flow over a flat plate and with a fully developed turbulent pipe flow.

In 1937, Egli (6) completed an investigation of the flow of air and steam through narrow channels. He obtained the result that the friction coefficient was a function of the length-clearance ratio as well as the Reynolds number and the roughness. For flow through a channel of a definite clearance, the friction coefficient decreased with each increase of the length-clearance ratio.

Keenan and Neumann (7) conducted an experimental investigation of apparent friction coefficients for the flow of air through smooth pipes at subsonic and supersonic velocities. The air streams were introduced into the test tubes through bellmouth entrances. Results of this investigation led to the conclusion that within an entry length of about 50 diameters, the apparent friction coefficient for supersonic flow was a function of the length-diameter ratio and the Reynolds number. It was found that at distances from the inlet greater than 50 diameters, the apparent friction coefficient for either subsonic or supersonic flow is approximately equal, for equal Reynolds numbers, to the coefficient for incompressible flow with fully developed boundary layer. It was further concluded that the variation of the friction coefficient with the length-diameter ratio at supersonic flow was similar to the variation corresponding to incompressible flow. However, the investigators agreed that an

accurate comparison could not be made because insufficient data were available for incompressible flow through the inlet length.

In 1947, Shapiro and Smith (8) completed an experimental study of apparent friction coefficients in the inlet length of smooth, round tubes with bellmouth entrances. They conducted the tests with the flow of water and air at Reynolds numbers corresponding to fully developed turbulent flow. Values of the coefficients determined from these tests were reported in terms of both local apparent friction coefficients and integrated apparent friction coefficients. The integrated friction coefficient is a measure of the total pressure loss from the inlet to the point involved. Values of the local coefficients were compared with the Karman-Nikuradse coefficient for fully developed flow, the theory of Langhaar, and the flat plate theory.

Near the inlet, the tests indicated a zone of laminar boundary layer, followed by a region in which the boundary layer was turbulent. Transition from laminar to turbulent boundary layer was found to occur at a Reynolds number (based on distance from the tube inlet) of about 5×10^5, which compares well with the corresponding value for a flat plate. In the laminar inlet zone, the apparent friction coefficient was found to decrease rapidly with increasing length-diameter ratios. Then, a sharp increase accompanied the change from the laminar to the turbulent boundary layer. After some irregular variations, which were probably the result of adjustments of velocity profile within the boundary layer, the values of the coefficient approached the Karman-Nikuradse coefficient.

Within the laminar inlet zone, the reported values of the local apparent friction coefficient varied from 3.5 to 0.5 times the Karman-

Nikuradse coefficient. The investigators were of the opinion that very near the inlet it was probable that the apparent friction coefficient was infinite compared with the Karman-Nikuradse coefficient.

Values of the local apparent friction coefficient varied in the turbulent inlet zone from 1.5 to 0.8 times the Karman-Nikuradse coefficient. For the local and the integrated apparent friction coefficients to remain within five per cent of the Karman-Nikuradse value, about 50 tube diameters and 80 tube diameters respectively were required.

In addition to comparing well with the theory of flow over a flat plate, the pressure drop results of these tests were in agreement with predictions from Langhaar's laminar inlet theory.

The investigation by Shapiro and Smith seems to be the most recent in regard to friction coefficients in the length of transition. However, due to the limited data available, it appears that much additional experimental work must be completed before definite conclusions may be advanced with confidence.

CHAPTER II

APPARATUS

A flow diagram of the apparatus used in this investigation is given in figure 26. Figures 29 and 30 are photographs of the test apparatus.

The water used for all tests was obtained from a line supplied by a centrifugal pump at a pressure of approximately 60 psig. Water was drawn from the supply line, through a globe valve, through the calming chamber to the test pipe, and, after passing through the test pipe and a second globe valve, was discharged into an open weighing tank.

In order to obtain the desired conditions of uniform velocity and minimum turbulence in the flow at the inlet of the test tube, a calming chamber ten inches in diameter and four feet eight inches in length was placed upstream of the test tube. It was believed that this calming chamber with its baffle, tube bundle and screens as shown in figure 28 would reduce the initial turbulence in the test section to small proportions. Also, the large ratio of area reduction between the chamber and test tubes would further promote uniform flow. The baffle consisted of sheet brass with one-inch holes drilled so as to distribute the flow over the entire cross section of the calming chamber. Two-foot lengths of one and one-quarter inch pipe were filed smooth, painted with a waterproofing paint, and placed inside the calming chamber to form the tube bundle. Two brass screens were installed downstream to remove turbulence produced by the tube bundle.

A Y-type filter was installed in the line before the calming chamber in order to protect the apparatus from excess foreign matter.

Each test tube was attached to the calming chamber by a bellmouth entry section machined from brass to very close tolerances. In each case, the inlet curve was a circular arc with a radius equal to the diameter of the test tube. Cross sections of the three entry sections are shown in figure 27. Each bellmouth entry was attached to the test tube with soft solder and the inlet curve burnished so that there was no observable junction between the bellmouth and the tube.

The three test tubes were one-half inch, three-quarter inch and one inch Type L straight drawn copper tubing approximately one-hundred diameters in length. Pressure taps were located at distances from the inlet as indicated in table 23. Because of the emphasis on the region of changing velocity profile, the pressure taps were more closely spaced near the inlet. These pressure taps were drilled through the tube wall and great care was exercised to insure that they were free of burrs. Actually, the inside of each tube was burnished with very fine polishing cloth after the taps were drilled. Connections were made to the pressure taps by means of three-inch lengths of one-quarter inch copper tubing soldered to the outside wall of the test tube.

Each pressure tap was connected through one-quarter inch copper tubing and shutoff valves to two pressure manifolds arranged so that any tap could be connected to either leg of three different manometers used in the test. Therefore, pressure differences between any two taps could be measured on any one of the three manometers. Also, the taps could be

reversed relative to the manifolds and the manometers, thus affording a test for leakage and a check on readings.

The three manometers used were a mercury-water U-tube manometer, a vertical air-water manometer and an air-water manometer inclined at an angle of 11° 32' (sine θ = 0.200). The two air-water manometers were constructed so as to permit application of a common air pressure to the top of each leg. The pressure manifolds were connected to the bottom of each manometer tube. Therefore, upon application of water pressure, the water level in the tube would rise until the total head was equalized by the air pressure. Thus, the difference in height of the two columns of water indicated the pressure drop between taps. The air pressure applied to the manometer was controlled by a regulator.

Initially, a mercury micromanometer was installed to measure the very small pressure differences. However, after numerous unsuccessful attempts to measure the small pressure drops at low rates of flow through the one inch tube, it was decided that the use of an inclined air-water manometer would result in more accurate data.

CHAPTER III

TEST PROCEDURE

To initiate a test, the supply valve and the discharge valve were regulated to permit the desired rate of flow. This procedure entailed purging the calming chamber of air, partially opening the discharge valve, and then adjusting the supply valve to establish a prescribed constant pressure within the calming chamber. The water flowing through the apparatus was then weighed by discharging into an open tank. This procedure was repeated until the desired rate of flow was established. After the steady flow rate had been established, the pressure taps, manifolds, manometers, and all connecting lines were purged of air. This was accomplished by removing the plug located above the manometers, and, by opening the shutoff valves, allowing water to flow for an adequate length of time through each manifold and through each leg of the air-water manometers. Air was removed from the lines to the water-mercury manometer by loosening the connections at the top of the manometer.

With two pressure tap shutoff valves open to opposite manifolds, air pressure was applied to the lines above the air-water manometers, thus forcing the water level down into the legs of the manometers. Sufficient time was allowed for all droplets of water to drain into the manometer tubes and all entrained air bubbles were removed from the columns of water. Subsequently, precautions were taken to prevent the water levels from dropping and entraining air in the manifolds at the bottom of the manometers.

However, the purging operation was repeated whenever the water level in either leg dropped into the manifold.

After the purging procedure, the rate of flow was again checked by weighing the discharge for the period of time necessary to fill the weighing tank to its capacity of approximately five hundred pounds. This concluded the operations preparatory to the actual observation of data.

The exact testing procedure varied with the different tests, but in general as many measurements as possible were made with the inclined manometer. Then, as the pressure differences increased beyond range of the inclined manometer, readings were taken from the vertical air-water manometer and finally the larger differences were measured with the mercury manometer.

To measure the pressure drop between any two points, the taps were opened to opposite pressure manifolds by means of the tap shutoff valves. Then, by means of the manometer shutoff valves, the manifolds were opened to opposite legs of the appropriate manometer. After observing the pressure difference, the taps were reversed relative to the manifolds and a second value for the pressure drop was recorded.

In an effort to increase the accuracy of the observed data, the pressure drops were measured and recorded in an accumulative manner whenever possible. For example, pressure drops were measured between taps one and two, one and three, one and four, and so on until restricted by the range of the manometer. In the same manner, subsequent downstream measurements were recorded relative to other selected taps. Because of the fact that equalization of the air pressure and the water pressure resulted in fluctuations of the water levels within the manometer tubes, all

measurements were read from the air-water manometers by two observers.

Throughout the test, the pressure within the calming chamber was closely observed and maintained constant by either opening or closing the supply valve by very small increments. Also, the temperature of the water flowing through the apparatus was observed frequently throughout the test and the average value recorded.

CHAPTER IV

DISCUSSION

The results of the tests are given in figures 1 through 22 in the form of curves in which the local apparent friction coefficients and the integrated apparent friction coefficients are plotted against the length/diameter ratio. The results of each test were plotted in a separate figure. Also, in figures 23 through 25, values of the local apparent friction coefficient are plotted against values of R_X (Reynolds number based on distance from the inlet). For purposes of comparison, the values of friction coefficients according to the theory of Langhaar and the values according to the theory of laminar and turbulent flow over a flat plate are also plotted.

Tube I.--For flow at low values of R_D, the results indicate that the boundary layer is initially laminar with a subsequent change to a turbulent boundary layer. For tests A and B, it will be observed from figures 1 and 2 that initially the values of the local apparent friction coefficient decrease rapidly to a minimum. After some fluctuations, the values increase sharply at L/D values of ten and seven for tests A and B respectively. When plotted in figure 23, the results of tests A, B, and C indicated that transition from laminar to turbulent boundary layer occurred at values of R_X between 4×10^5 and 6×10^5.

In regard to the higher rates of flow, figure 23 indicates that for tests E and F, the boundary layer is turbulent from the beginning of

the observed inlet length. The results for tests D and G are similar to those for tests E and F. As represented in figures 4, 5, 6, and 7, the local apparent friction coefficients for tests D, E, F, and G decrease rapidly from very high initial values. Since it has been indicated that this decrease occurs within the zone of turbulent boundary layer, it therefore follows that turbulence greatly increases the apparent friction coefficient in the region that would normally be the laminar inlet zone. This fact is supported by results obtained by Shapiro and Smith. For a test with water flow, they found that turbulence induced by a wire screen at the tube inlet resulted in a threefold increase in the region where R_x is less than 5×10^5. Similarly, for air flow, a strip of tape placed on the tube wall at its entrance caused an eightfold increase in the coefficient. Shapiro and Smith further concluded that initial turbulence either moves forward the point of transition from laminar to turbulent boundary layer or entirely eliminates the laminar region.

Pressure drop data definitely indicate that the bellmouth entrance section induced an undetermined amount of turbulence at the high rates of flow. This explanation is given for the fact that pressure increases were recorded between taps one and two, two and three, and four and five for tests D, E, F, and G. Therefore, as evidenced by figure 23, the normally laminar boundary layer was displaced by a turbulent boundary layer at high rates of flow.

After the initial peak following transition to turbulent boundary layer, it was anticipated that the value of the friction coefficient would gradually decrease, with small fluctuations, and approach the value of the Karman-Nikuradse coefficient. The values for test A followed this expected

pattern. However, for tests B through G, the values of the coefficients varied widely within the region of L/D values from 15 to 50. As indicated in figures 1 through 7, high maximum values were recorded at L/D ratios of 20 and 38. It was believed that the effects of the entrance section probably contributed to these wide variations.

Values of the integrated friction coefficients approached the Karman-Nikuradse coefficient in tests A and B, and exhibited trends toward the Karman-Nikuradse value in tests C through G. If the length of the test tube had been greater, values of the integrated coefficient for all tests certainly would have approached the corresponding values of the Karman-Nikuradse coefficient. In general, the integrated friction coefficient at any L/D value is greater than the Karman-Nikuradse value when the Reynolds number exceeds 150,000. When the Reynolds number is less than 150,000, the integrated coefficient is less than the Karman-Nikuradse value for low values of the L/D ratio and greater than the Karman-Nikuradse value for the higher values of the L/D ratio.

Tube II.--As in the case of Tube I, initial turbulence was introduced by the bellmouth entry; pressure increases were measured between taps four and five in all tests and between taps two and three in tests C through H. Figure 24 indicates that, for all tests, the boundary layer was turbulent from the beginning of the observed inlet length. Therefore, it was concluded that the initial increase and subsequent decrease in the values of the friction coefficients between L/D ratios of 0.75 and 7.00 occurred in the region of turbulent boundary layer, thus resulting in the high values of the coefficients. Within the region of L/D values between 2.5 and 10.0,

the results of these tests were very similar to the results obtained for the high rates of flow through Tube I.

In general, values of the local apparent friction coefficients remain within about 20 per cent of the Karman-Nikuradse value beginning at ten diameters from the tube inlet. The integrated friction coefficients decrease from very high initial values and approach corresponding values of the Karman-Nikuradse coefficient in asymptotic fashion. Figure 24 indicates that after an R_x value of approximately 5×10^5, the results are similar to the theory of turbulent flow over a flat plate.

Tube III.--No pressure increases were recorded in any of the tests conducted with Tube III. Therefore, it was assumed that any initial turbulence would be of smaller proportion than that induced by the entrance sections of Tubes I and II. The smaller tube size together with the greater ratio of area reduction between the calming chamber and test tube would promote laminar flow at the tube entrance.

Figure 25 indicates that the initial region of the boundary layer was laminar with transition to a turbulent boundary layer at R_x values ranging from approximately 4.0×10^5 to 6.5×10^5. However, the test data indicated that the entrance section induced enough turbulence to cause an excessively high static pressure at the fourth tap. Accordingly, the observed pressure differences between taps three and four and between taps four and five were assumed to be respectively lower and higher than the differences which would have resulted if the velocity had been uniform at the inlet. Therefore, the resulting values of the friction coefficients at 2.5 diameters and at 3.5 diameters were respectively low and high. It was concluded that the initial turbulence thus contributed to the relative

high values of the coefficient at 3.5 diameters from the inlet. Considering the fact that actual pressure increases were recorded in Tests I and II, this condition could reasonably be expected.

Within the region of turbulent boundary layer, values of the local apparent friction coefficient varied from approximately 0.25 to 2.0 times the Karman-Nikuradse coefficient. These wide variations were believed to result from the effects of the entrance section. For all rates of flow, the integrated apparent friction coefficient initially decreased with increasing L/D ratios. Then, accompanying the transition to turbulent boundary layer, the coefficient increased to a maximum and subsequently decreased to approach the Karman-Nikuradse coefficient. Values of the integrated coefficients varied from approximately 0.70 to 1.50 times the Karman-Nikuradse value.

CHAPTER V

CONCLUSIONS

The following conclusions were drawn from the experimental investigation of friction coefficients in the inlet length of smooth, round tubes with bellmouth entrances.

1. It is the opinion of the writer that the bellmouth entrances used in the investigation did not result in uniform velocity distributions at the tube inlets.

2. The turbulence, although unexplained, induced by the entrance nozzle, acted either to move forward the point of transition from laminar to turbulent boundary layer or to eliminate the laminar boundary layer entirely.

3. For flow through Tube III and for flow through Tube I at R_D values less than 125,000, the boundary layer was initially laminar with transition to turbulent boundary layer at an average R_X value of about 500,000.

4. For flow through Tube II and for flow through Tube I at R_D values greater than 125,000, the boundary layer was turbulent from the beginning of the observed inlet length.

5. Within the region of laminar boundary layer, the local apparent friction coefficient decreased with increasing distance from the tube inlet.

6. A sharp increase in the friction coefficient accompanied the transition from laminar to turbulent boundary layer.

7. Initial turbulence tended to increase the magnitude of the variations in the values of friction coefficients within the zone of turbulent boundary layer.

8. Elimination of the laminar boundary layer by induced turbulence acted to greatly increase the value of the apparent friction coefficient in the region which would normally be the laminar inlet zone.

9. Due to the variations in the observed data, no definite value of the inlet length could be accurately determined.

CHAPTER VI

RECOMMENDATIONS

There is a great need for compilation of experimental data on friction coefficients in the inlet length of round tubes. In the case of tests conducted with turbulent flow, the foremost problem seems to be that of securing a uniform velocity distribution at the tube inlet. Therefore, further investigations should be made with improved combinations of approach sections and tube entrances. The need of velocity probes as a means of evaluating profiles is indicated.

Considering the data of this thesis, better results may be obtained by the use of a bell mouth entrance designed with an inlet curve of greater radius. Also, a larger calming chamber would tend to reduce the amount of initial turbulence.

In order to more accurately determine values of the friction coefficient, it seems advisable to install a larger number of pressure taps; or consideration might be given to determination of local friction factors by measurement of the wall shear stress and probes of the velocity profile.

APPENDIX A

EXPERIMENTAL RESULTS

Table 1. Test A, Tube I.

P_{cc} = 26 psig R_D = 54,100

W_w = 115 lbs./min. f_{K-N} = 0.0206

T_w = 88° F.

Pressure Taps	ΔP ("H_2O)	f_{APP}	f_{APP}/F_{K-N}	$\bar{f}_{APP}$	$\bar{f}_{APP}/f_{K-N}$
1-2	0.06	0.0225	1.09	0.0225	1.09
2-3	0.06	0.0225	1.09	0.0225	1.09
3-4	0.08	0.0300	1.45	0.0240	1.16
4-5	0.06	0.0113	0.55	0.0216	1.05
5-6	0.06	0.0113	0.55	0.0181	0.88
6-7	0.12	0.0113	0.55	0.0158	0.77
7-8	0.16	0.0150	0.73	0.0150	0.73
8-9	0.22	0.0131	0.64	0.0146	0.71
9-10	0.54	0.0253	1.23	0.0160	0.78
10-11	1.00	0.0234	1.15	0.0185	0.90
11-12	0.90	0.0211	1.02	0.0196	0.95
12-13	1.70	0.0225	1.09	0.0208	1.01
13-14	1.80	0.0211	1.02	0.0216	1.05
14-15	1.50	0.0176	0.86	0.0210	1.02
15-16	2.40	0.0225	1.09	0.0209	1.01

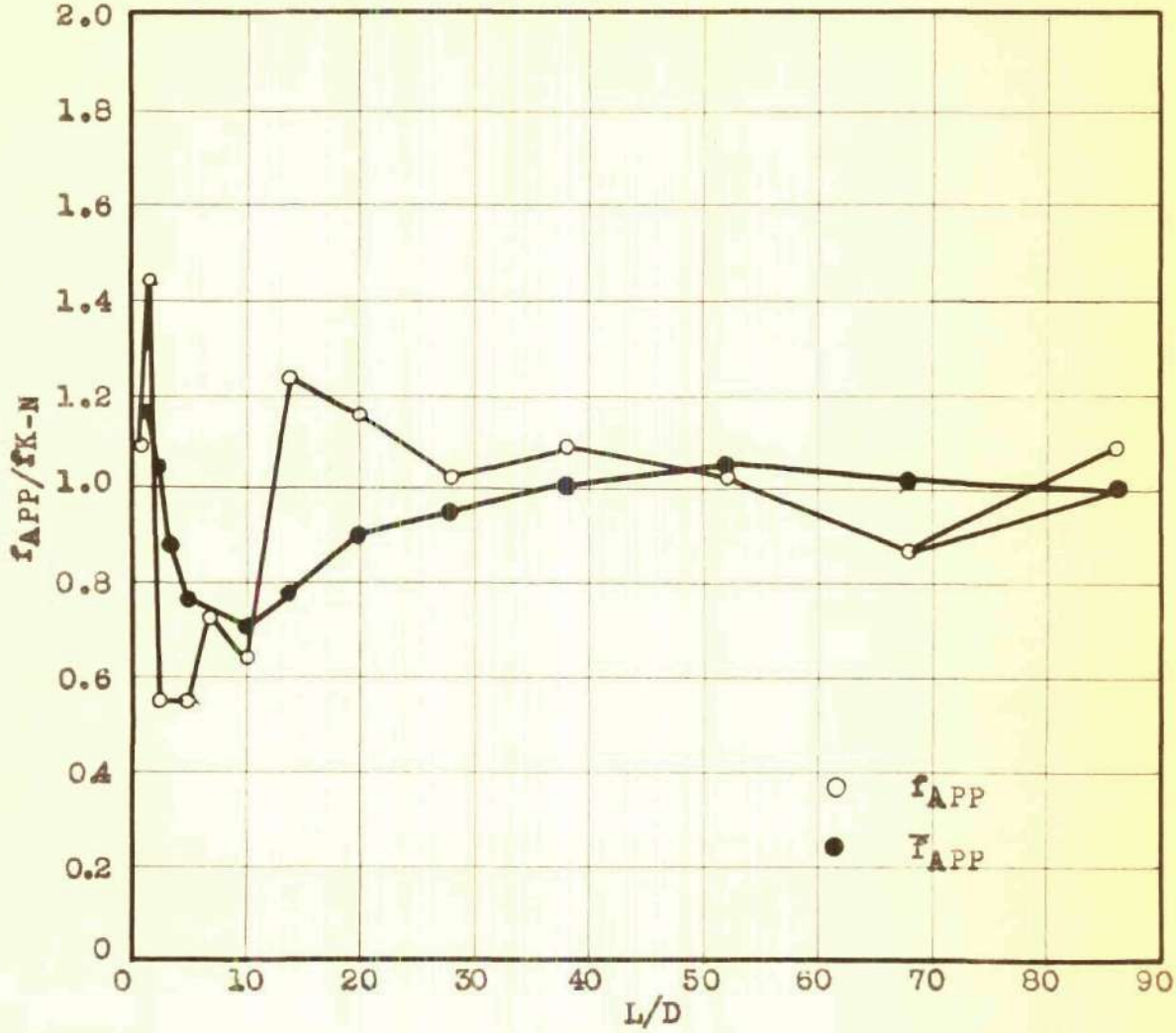

Figure 1. Results for Test A, Tube I. Ratios of local and integrated apparent friction coefficients to the Karman-Nikuradse friction coefficient against L/D for constant value of R_D.

Table 2. Test B, Tube I.

P_{cc} = 25 psig R_D = 78,300

W_w = 172 lbs./min. f_{K-N} = 0.0190

T_w = 85° F.

Pressure Taps	ΔP ("H_2O)	f_{APP}	f_{APP}/f_{K-N}	$\overline{f}_{APP}$	$\overline{f}_{APP}/f_{K-N}$
1-2	0.12	0.0202	1.06	0.0202	1.06
2-3	0.04	0.0067	0.35	0.0157	0.83
3-4	0.04	0.0067	0.35	0.0121	0.64
4-5	0.16	0.0134	0.70	0.0117	0.62
5-6	0.20	0.0168	0.88	0.0129	0.68
6-7	0.24	0.0101	0.53	0.0127	0.67
7-8	0.24	0.0101	0.53	0.0119	0.63
8-9	1.08	0.0221	1.19	0.0140	0.74
9-10	0.98	0.0201	1.08	0.0162	0.85
10-11	2.30	0.0241	1.27	0.0183	0.96
11-12	1.60	0.0168	0.88	0.0189	1.00
12-13	4.20	0.0294	1.55	0.0203	1.07
13-14	2.70	0.0142	0.75	0.0204	1.07
14-15	3.40	0.0178	0.94	0.0194	1.02
15-16	4.50	0.0189	0.99	0.0192	1.01

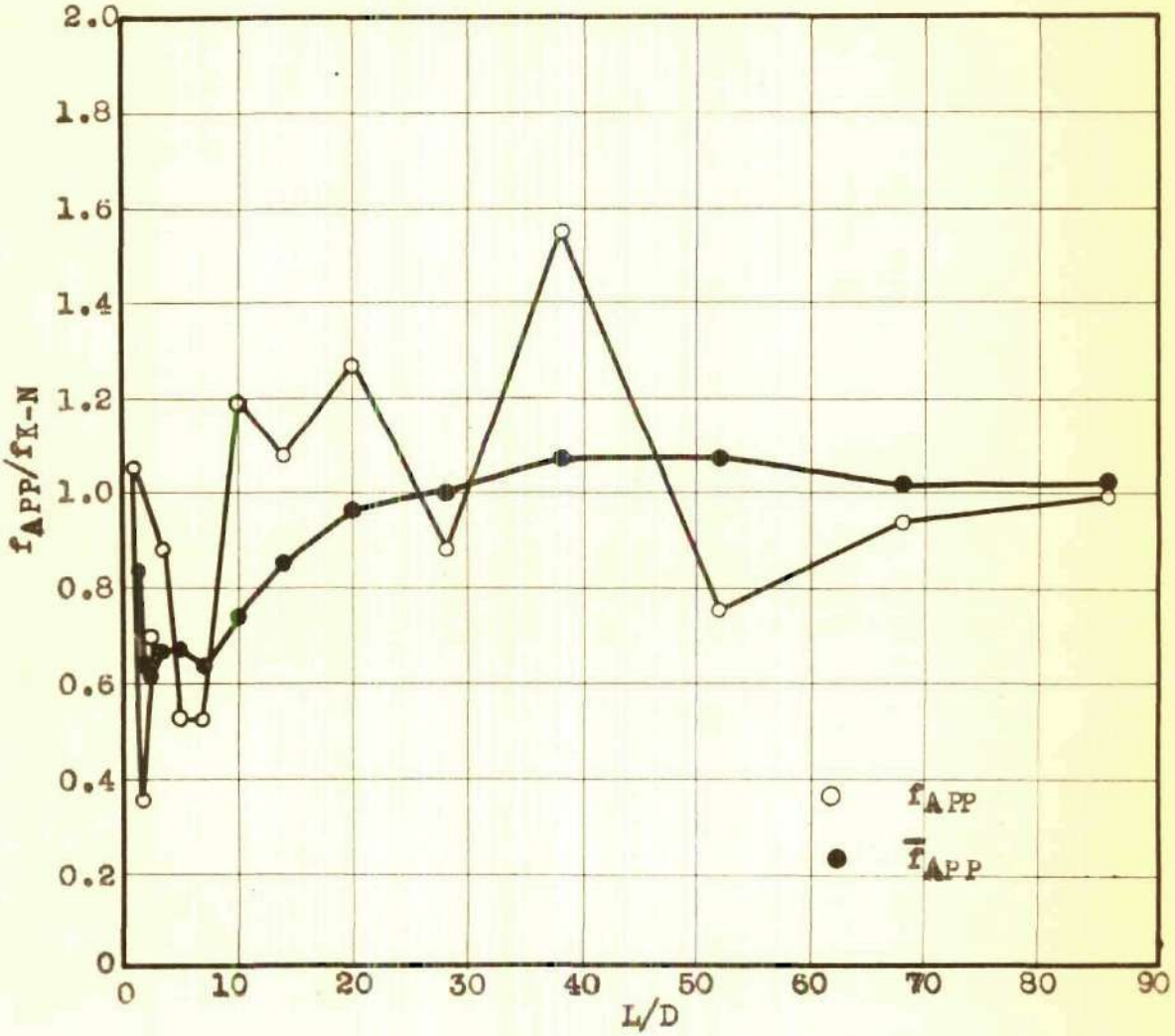

Figure 2. Results for Test B, Tube I. Ratios of local and integrated apparent friction coefficients to the Karman-Nikuradse friction coefficient against L/D for a constant value of R_D.

Table 3. Test C, Tube I.

P_{cc} = 26 psig

W_w = 215 lbs./min.

T_w = 88° F.

R_D = 101,200

f_{K-N} = 0.0179

Pressure Taps	ΔP ("H_2O)	f_{APP}	f_{APP}/f_{K-N}	$\overline{f}_{APP}$	$\overline{f}_{APP}/f_{K-N}$
1-2	0.08	0.0086	0.48	0.0086	0.48
2-3	0.04	0.0043	0.24	0.0072	0.40
3-4	0.12	0.0129	0.72	0.0077	0.43
4-5	0.06	0.0032	0.18	0.0073	0.41
5-6	0.20	0.0108	0.60	0.0072	0.40
6-7	0.56	0.0150	0.84	0.0093	0.52
7-8	0.64	0.0172	0.96	0.0114	0.64
8-9	1.80	0.0242	1.35	0.0147	0.82
9-10	1.50	0.0202	1.13	0.0169	0.94
10-11	3.70	0.0248	1.39	0.0189	1.06
11-12	2.70	0.0181	1.01	0.0196	1.10
12-13	6.50	0.0291	1.63	0.0210	1.17
13-14	5.00	0.0168	0.94	0.0213	1.19
14-15	5.00	0.0168	0.94	0.0202	1.13
15-16	8.80	0.0236	1.32	0.0202	1.13

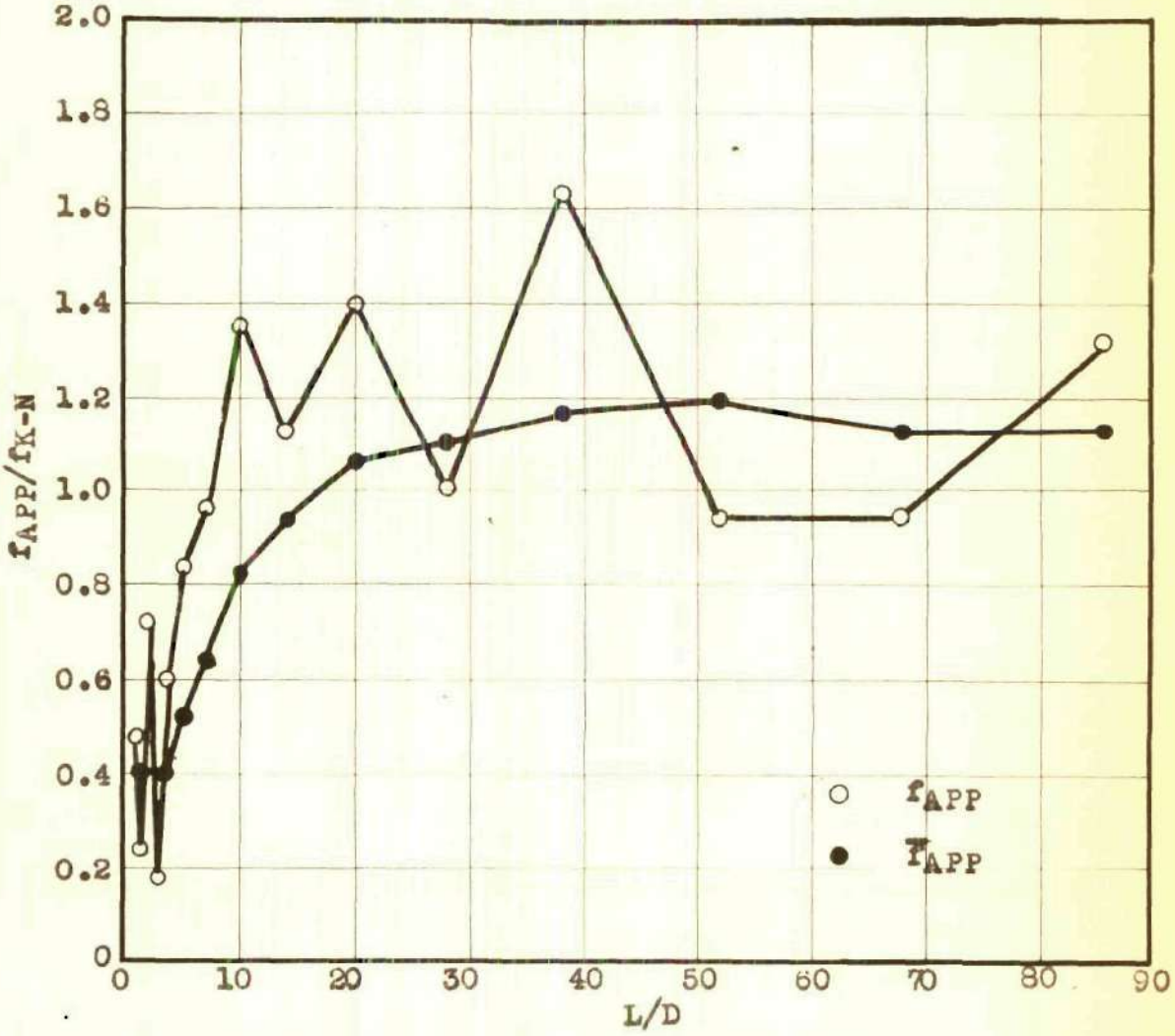

Figure 3. Results for Test C, Tube I. Ratios of local and integrated apparent friction coefficients to the Karman-Nikuradse friction coefficient against L/D for a constant value of R_D.

Table 4. Test D, Tube I.

P_{cc} = 25 psig

W_w = 271 lbs./min.

T_w = 86° F.

R_D = 125,000

f_{K-N} = 0.0172

Pressure Taps	ΔP ("H_2O)	f_{APP}	f_{APP}/f_{K-N}	$\bar{f}_{APP}$	$\bar{f}_{APP}/f_{K-N}$
1-2	0.14	0.0095	0.55	0.0095	0.55
2-3	+0.06	--	--	--	--
3-4	0.58	0.0392	2.28	0.0116	0.67
4-5	+0.14	--	--	--	--
5-6	0.50	0.0169	0.98	0.0109	0.63
6-7	1.08	0.0182	1.06	0.0132	0.77
7-8	1.10	0.0186	1.08	0.0143	0.83
8-9	2.70	0.0220	1.28	0.0169	0.98
9-10	2.10	0.0177	1.03	0.0179	1.04
10-11	5.90	0.0250	1.45	0.0193	1.12
11-12	3.50	0.0148	0.86	0.0195	1.13
12-13	11.5	0.0324	1.88	0.0210	1.22
13-14	6.10	0.0128	0.75	0.0211	1.23
14-15	8.55	0.0181	1.05	0.0198	1.15
15-16	10.9	0.0184	1.07	0.0195	1.13

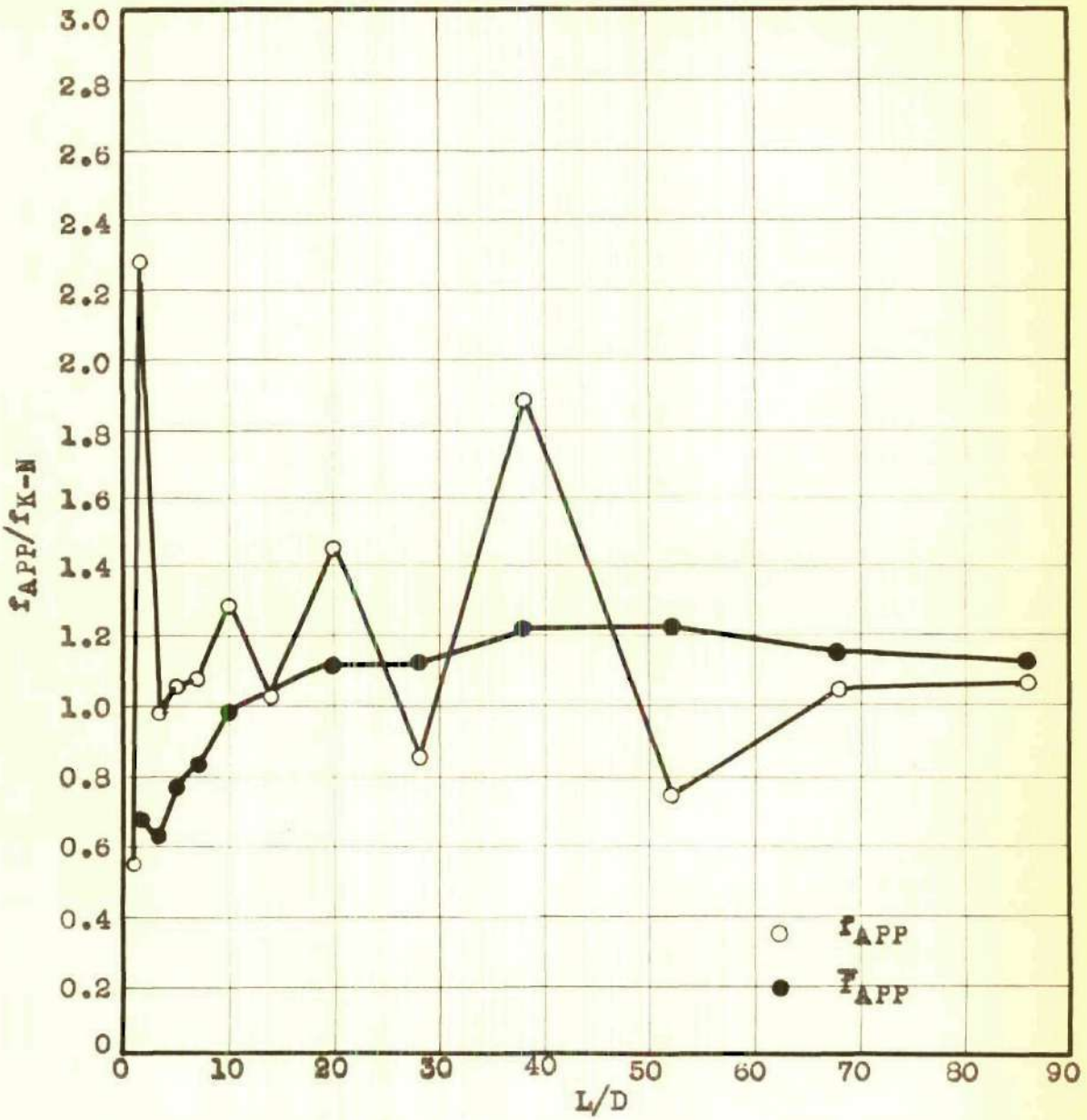

Figure 4. Results for Test D, Tube I. Ratios of local and integrated apparent friction coefficients to the Karman-Nikuradse friction coefficient against L/D for a constant value of R_D.

Table 5. Test E, Tube I.

P_{cc} = 24 psig

W_w = 326 lbs./min.

T_w = 88° F.

R_D = 153,500

f_{K-N} = 0.0165

Pressure Taps	ΔP ("H_2O)	f_{APP}	f_{APP}/f_{K-N}	$\overline{f}_{APP}$	$\overline{f}_{APP}/f_{K-N}$
1-2	0.00	--	--	--	--
2-3	+0.10	--	--	--	--
3-4	1.00	0.0468	2.84	0.0468	2.84
4-5	+0.50	--	--	--	--
5-6	0.80	0.0187	1.13	0.0164	0.99
6-7	1.34	0.0157	0.95	0.0165	1.00
7-8	1.96	0.0230	1.39	0.0175	1.06
8-9	3.40	0.0199	1.21	0.0187	1.13
9-10	3.20	0.0187	1.13	0.0189	1.14
10-11	7.80	0.0228	1.38	0.0197	1.19
11-12	5.00	0.0146	0.89	0.0194	1.18
12-13	14.9	0.0291	1.76	0.0205	1.24
13-14	10.2	0.0149	0.90	0.0206	1.25
14-15	10.2	0.0149	0.90	0.0197	1.19
15-16	16.3	0.0191	1.16	0.0188	1.14

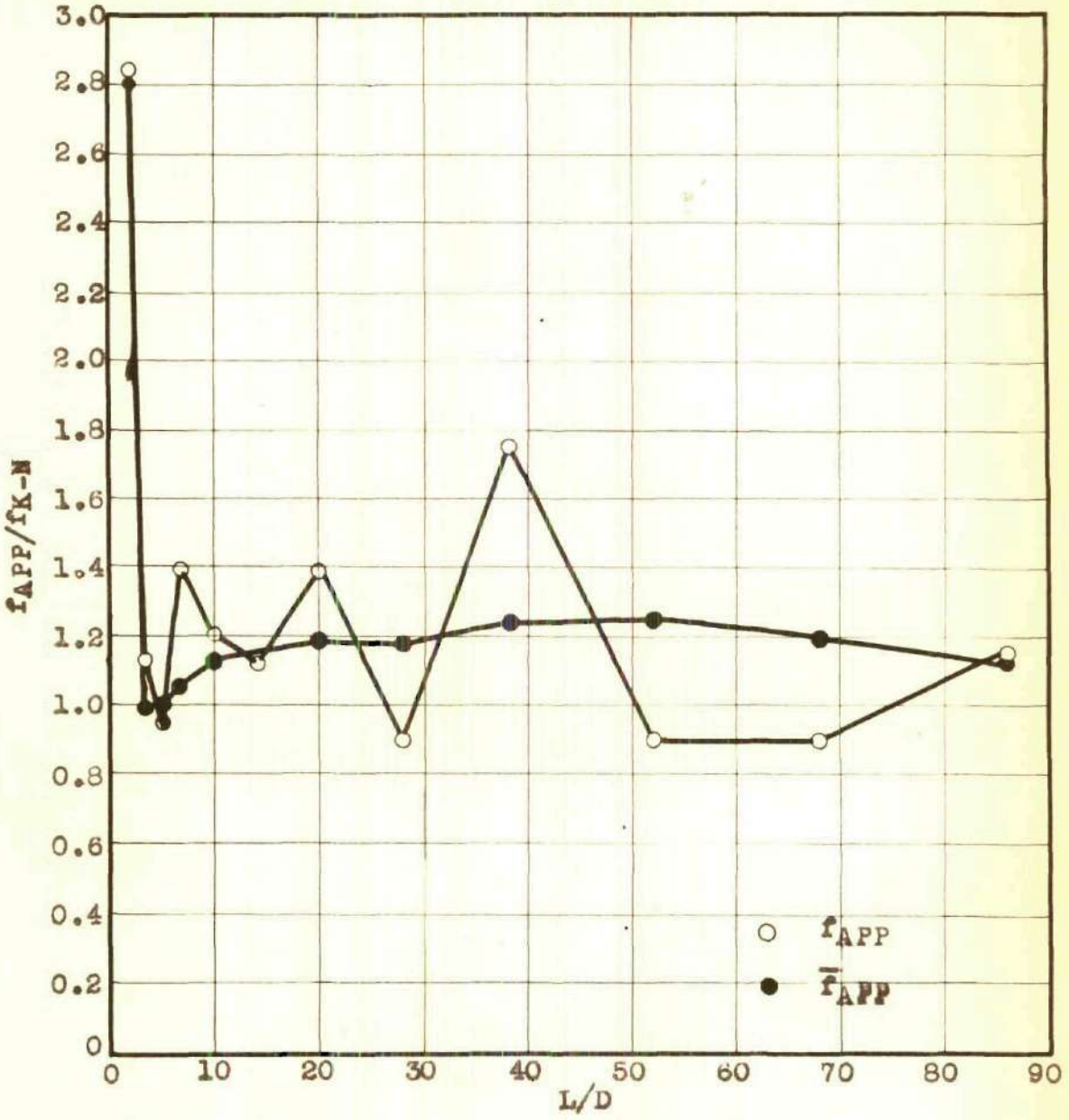

Figure 5. Results for Test E, Tube I. Ratios of local and integrated apparent friction coefficients to the Karman-Nikuradse friction coefficient against L/D for a constant value of R_D.

Table 6. Test F, Tube I.

P_{cc} = 23 psig

W_w = 474 lbs./min.

T_w = 88° F.

R_D = 223,000

f_{K-N} = 0.0153

Pressure Taps	ΔP ("H_2O)	f_{APP}	f_{APP}/f_{K-N}	$\overline{f}_{APP}$	$\overline{f}_{APP}/f_{K-N}$
1-2	+0.40	--	--	--	--
2-3	+0.50	--	--	--	--
3-4	2.90	0.0645	4.21	0.0645	4.21
4-5	+0.70	--	--	--	--
5-6	2.70	0.0300	1.96	0.0236	1.54
6-7	4.60	0.0255	1.67	0.0250	1.63
7-8	2.40	0.0133	0.88	0.0230	1.50
8-9	7.00	0.0194	1.27	0.0210	1.37
9-10	5.80	0.0161	1.05	0.0200	1.31
10-11	19.5	0.0270	1.76	0.0211	1.38
11-12	10.2	0.0141	0.92	0.0209	1.37
12-13	35.2	0.0326	2.13	0.0221	1.44
13-14	17.6	0.0122	0.80	0.0218	1.42
14-15	23.1	0.0160	1.05	0.0199	1.30
15-16	31.8	0.0177	1.16	0.0193	1.26

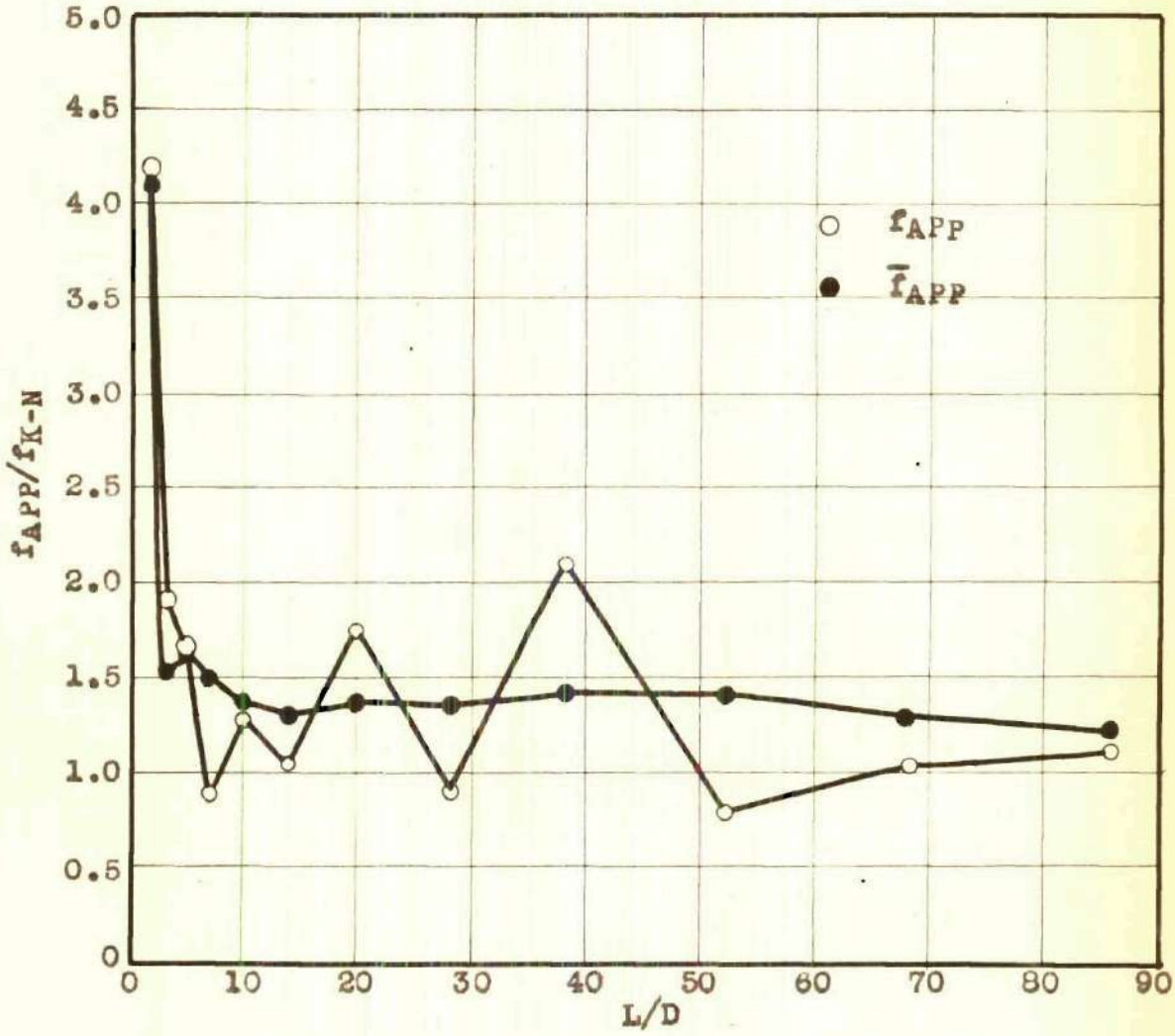

Figure 6. Results for Test F, Tube I. Ratios of local and integrated apparent friction coefficients to the Karman-Nikuradse friction coefficient against L/D for a constant value of R_D.

Table 7. Test G, Tube I.

P_{cc} = 30 psig

W_w = 610 lbs./min.

T_w = 89° F.

R_D = 290,000

f_{K-N} = 0.0146

Pressure Taps	ΔP ("H_2O)	f_{APP}	f_{APP}/f_{K-N}	$\bar{f}_{APP}$	$\bar{f}_{APP}/f_{K-N}$
1-2	+1.20	--	--	--	--
2-3	+1.00	--	--	--	--
3-4	7.80	0.1040	7.13	0.1040	7.13
4-5	+1.60	--	--	--	--
5-6	3.90	0.0260	1.78	0.0325	2.23
6-7	4.80	0.0160	1.10	0.0268	1.84
7-8	3.50	0.0117	0.80	0.0221	1.51
8-9	11.5	0.0192	1.31	0.0202	1.38
9-10	7.75	0.0129	0.88	0.0191	1.31
10-11	25.8	0.0214	1.47	0.0188	1.29
11-12	14.2	0.0118	0.81	0.0181	1.24
12-13	54.0	0.0300	2.06	0.0194	1.33
13-14	24.4	0.0102	0.70	0.0192	1.31
14-15	31.8	0.0132	0.90	0.0174	1.19
15-16	48.1	0.0144	0.99	0.0169	1.16

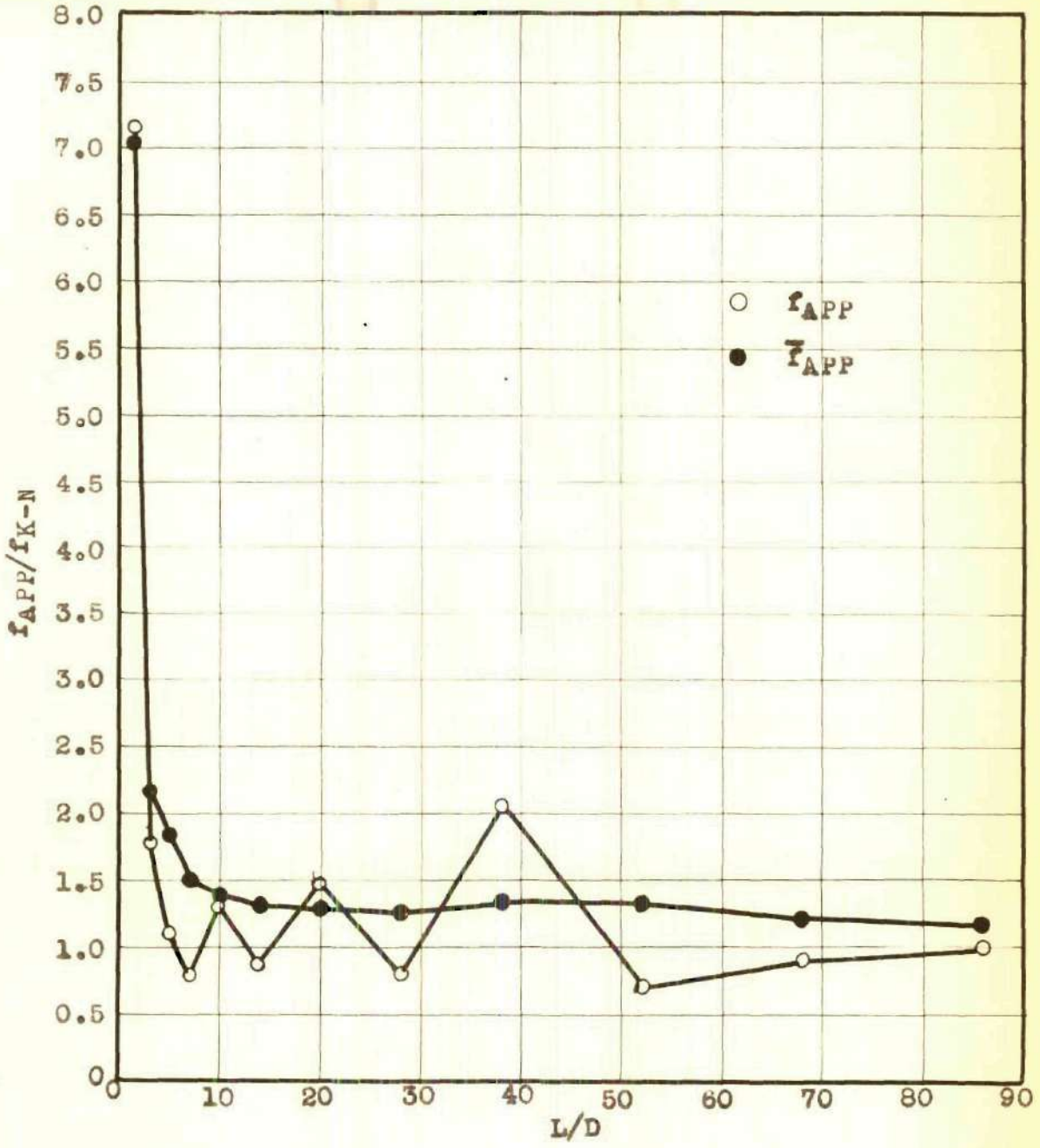

Figure 7. Results for Test G, Tube I. Ratios of local and integrated apparent friction coefficients to the Karman-Nikuradse friction coefficient against L/D for a constant value of R_D.

Table 8. Test A, Tube II

P_{cc} = 26 psig

W_w = 85 lbs./min.

T_w = 86° F.

R_D = 51,400

f_{K-N} = 0.0208

Pressure Taps	ΔP ("H_2O)	f_{APP}	f_{APP}/f_{K-N}	$\overline{f}_{APP}$	$\overline{f}_{APP}/f_{K-N}$
1-2	0.44	0.1030	4.95	0.1030	4.95
2-3	0.20	0.0234	1.13	0.0632	3.04
3-4	0.96	0.1120	5.39	0.0656	3.15
4-5	+0.70	--	--	--	--
5-6	0.34	0.0199	0.96	0.0461	2.22
6-7	0.16	0.0093	0.47	0.0364	1.75
7-8	0.84	0.0245	1.18	0.0309	1.48
8-9	0.80	0.0234	1.12	0.0290	1.39
9-10	1.66	0.0243	1.17	0.0274	1.32
10-11	1.50	0.0220	1.06	0.0262	1.26
11-12	2.30	0.0224	1.08	0.0251	1.20
12-13	3.60	0.0214	1.27	0.0250	1.20
13-14	2.65	0.0194	0.93	0.0245	1.18
14-15	3.70	0.0216	1.04	0.0238	1.14

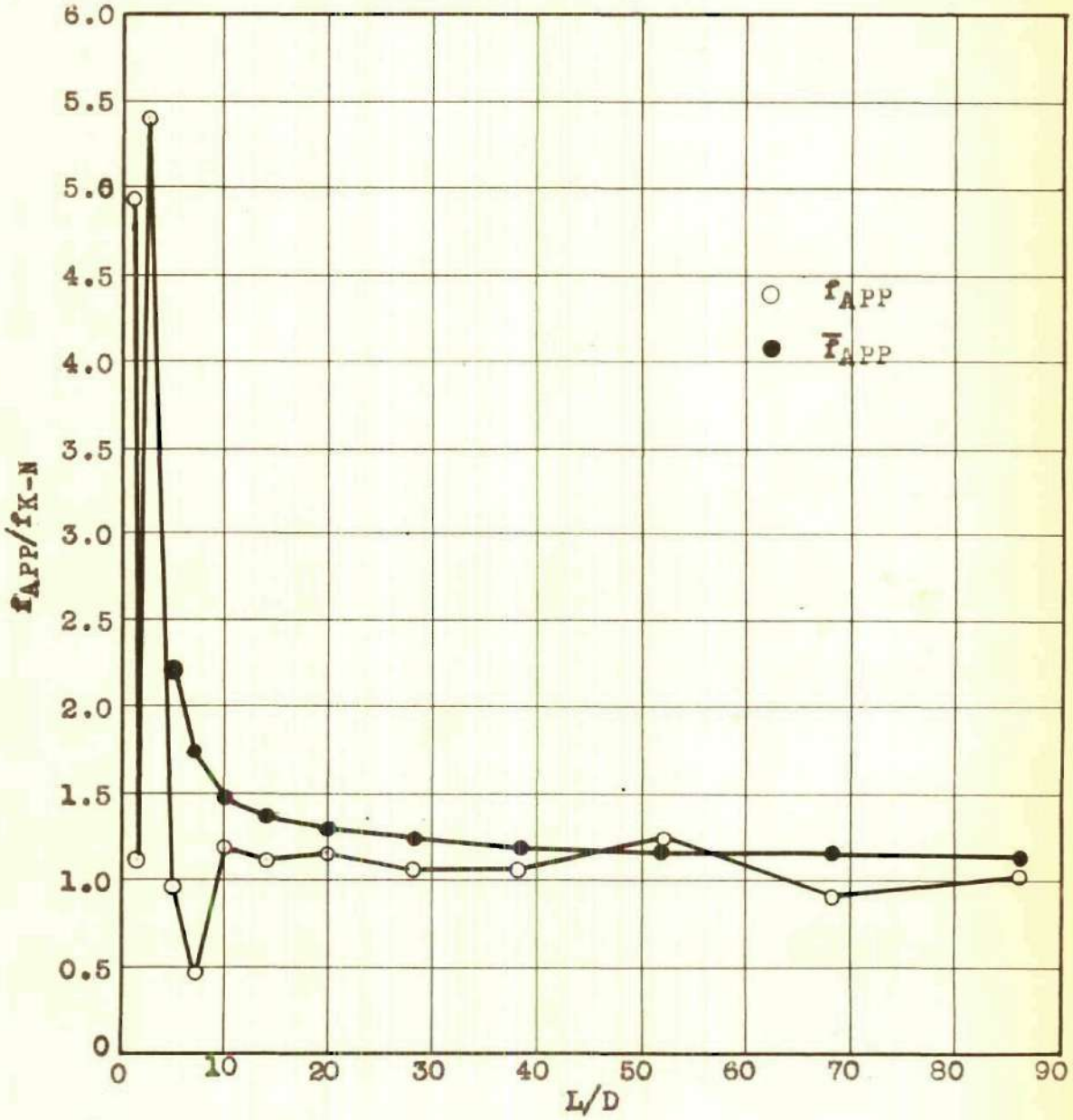

Figure 8. Results for Test A, Tube II. Ratios of local and integrated apparent friction coefficients to the Karman-Nikuradse friction coefficient against L/D for a constant value of R_D.

Table 9. Test B, Tube II.

P_{cc} = 25 psig

W_w = 121 lbs./min.

T_w = 86° F.

R_D = 73,000

f_{K-N} = 0.0192

Pressure Taps	ΔP ("H_2O)	f_{APP}	f_{APP}/f_{K-N}	$\overline{f}_{APP}$	$\overline{f}_{APP}/f_{K-N}$
1-2	0.80	0.0922	4.80	0.0922	4.80
2-3	0.28	0.0162	0.84	0.0542	2.82
3-4	2.32	0.1340	7.00	0.0646	3.36
4-5	+1.74	--	--	--	--
5-6	0.90	0.0260	1.35	0.0494	2.57
6-7	0.60	0.0173	0.90	0.0408	2.12
7-8	1.60	0.0231	1.20	0.0346	1.80
8-9	1.64	0.0236	1.23	0.0313	1.63
9-10	3.00	0.0216	1.12	0.0285	1.48
10-11	2.60	0.0188	0.98	0.0261	1.36
11-12	4.40	0.0211	1.10	0.0246	1.28
12-13	7.50	0.0271	1.41	0.0245	1.28
13-14	4.30	0.0155	0.81	0.0238	1.24
14-15	6.50	0.0188	0.98	0.0224	1.16

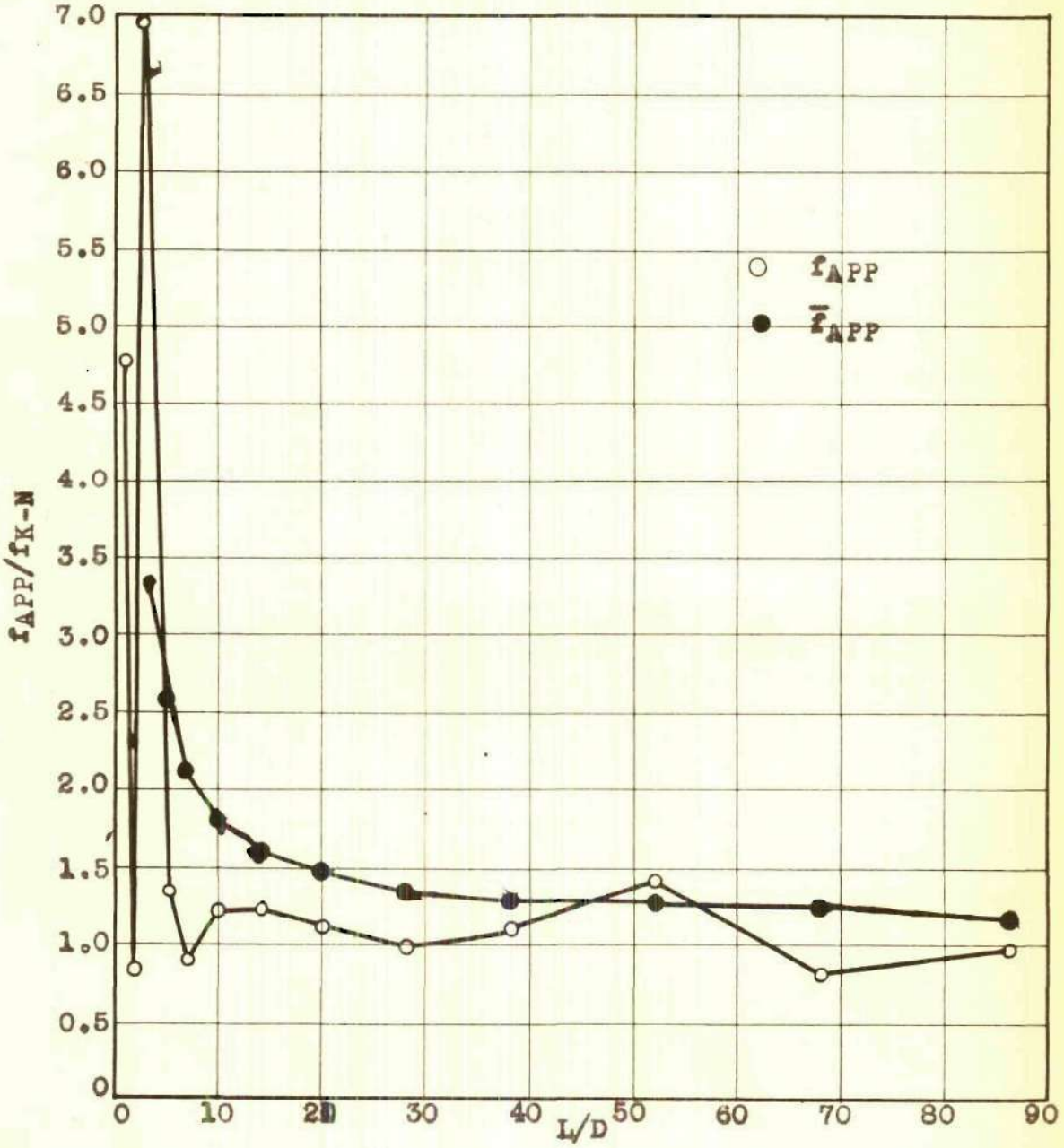

Figure 9. Results for Test B, Tube II. Ratios of local and integrated apparent friction coefficients to the Karman-Nikuradse friction coefficient against L/D for a constant value of R_D.

Table 10. Test C, Tube II.

P_{cc} = 26 psig

W_w = 165 lbs./min.

T_w = 88° F.

R_D = 101,500

f_{K-N} = 0.0179

Pressure Taps	ΔP ("H_2O)	f_{APP}	f_{APP}/f_{K-N}	$\bar{f}_{APP}$	$\bar{f}_{APP}/f_{K-N}$
1-2	1.34	0.0833	4.65	0.0833	4.65
2-3	+0.38	--	--	--	--
3-4	4.94	0.1535	8.58	0.0593	3.31
4-5	+3.00	--	--	--	--
5-6	1.66	0.0258	1.44	0.0492	2.74
6-7	1.18	0.0171	0.95	0.0407	2.27
7-8	2.84	0.0221	1.23	0.0342	1.91
8-9	2.50	0.0194	1.08	0.0303	1.69
9-10	5.20	0.0202	1.13	0.0271	1.51
10-11	4.60	0.0179	1.00	0.0258	1.39
11-12	7.80	0.0202	1.13	0.0233	1.30
12-13	8.70	0.0169	0.95	0.0220	1.23
13-14	10.2	0.0198	1.11	0.0211	1.18
14-15	11.3	0.0176	0.98	0.0205	1.14

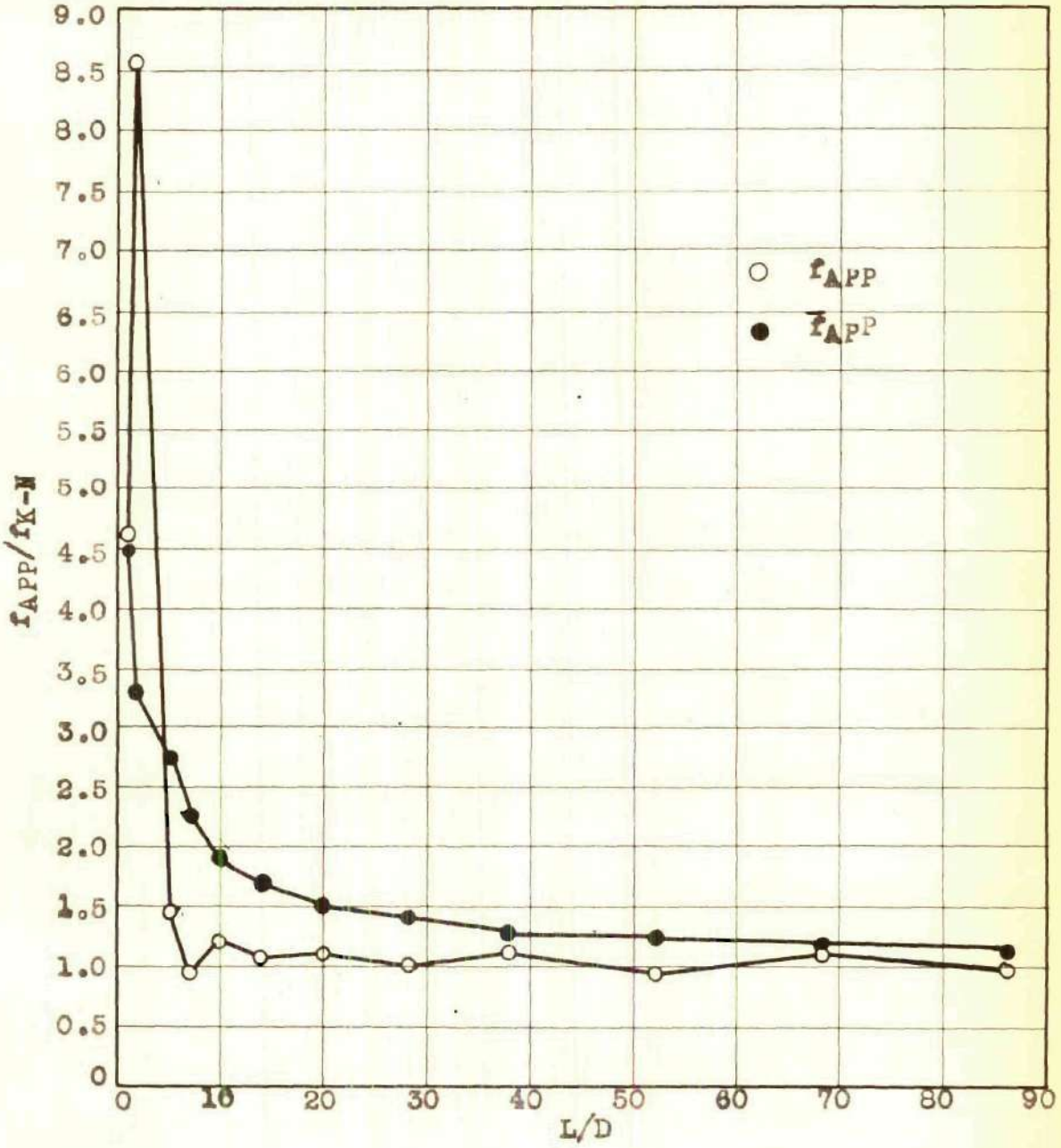

Figure 10. Results for Test C, Tube II. Ratios of local and integrated apparent friction coefficients to the Karman-Nikuradse friction coefficient against L/D for a constant value of R_D.

Table 11. Test D, Tube II.

P_{cc} = 24 psig

W_w = 212 lbs./min.

T_w = 88° F.

R_D = 130,500

f_{K-N} = 0.0170

Pressure Taps	ΔP ("H_2O)	f_{APP}	f_{APP}/f_{K-N}	$\bar{f}_{APP}$	$\bar{f}_{APP}/f_{K-N}$
1-2	2.20	0.0827	4.86	0.0827	4.86
2-3	+0.80	--	--	--	--
3-4	8.30	0.1560	9.18	0.0597	3.51
4-5	+4.80	--	--	--	--
5-6	3.70	0.0348	2.04	0.0516	3.04
6-7	1.10	0.0103	0.61	0.0427	2.51
7-8	3.80	0.0179	1.05	0.0340	2.00
8-9	4.10	0.0193	1.13	0.0295	1.73
9-10	8.50	0.0200	1.18	0.0265	1.56
10-11	7.40	0.0174	1.02	0.0242	1.42
11-12	11.6	0.0182	1.07	0.0225	1.32
12-13	13.3	0.0156	0.92	0.0209	1.23
13-14	17.0	0.0200	1.18	0.0202	1.19
14-15	18.5	0.0174	1.02	0.0197	1.16

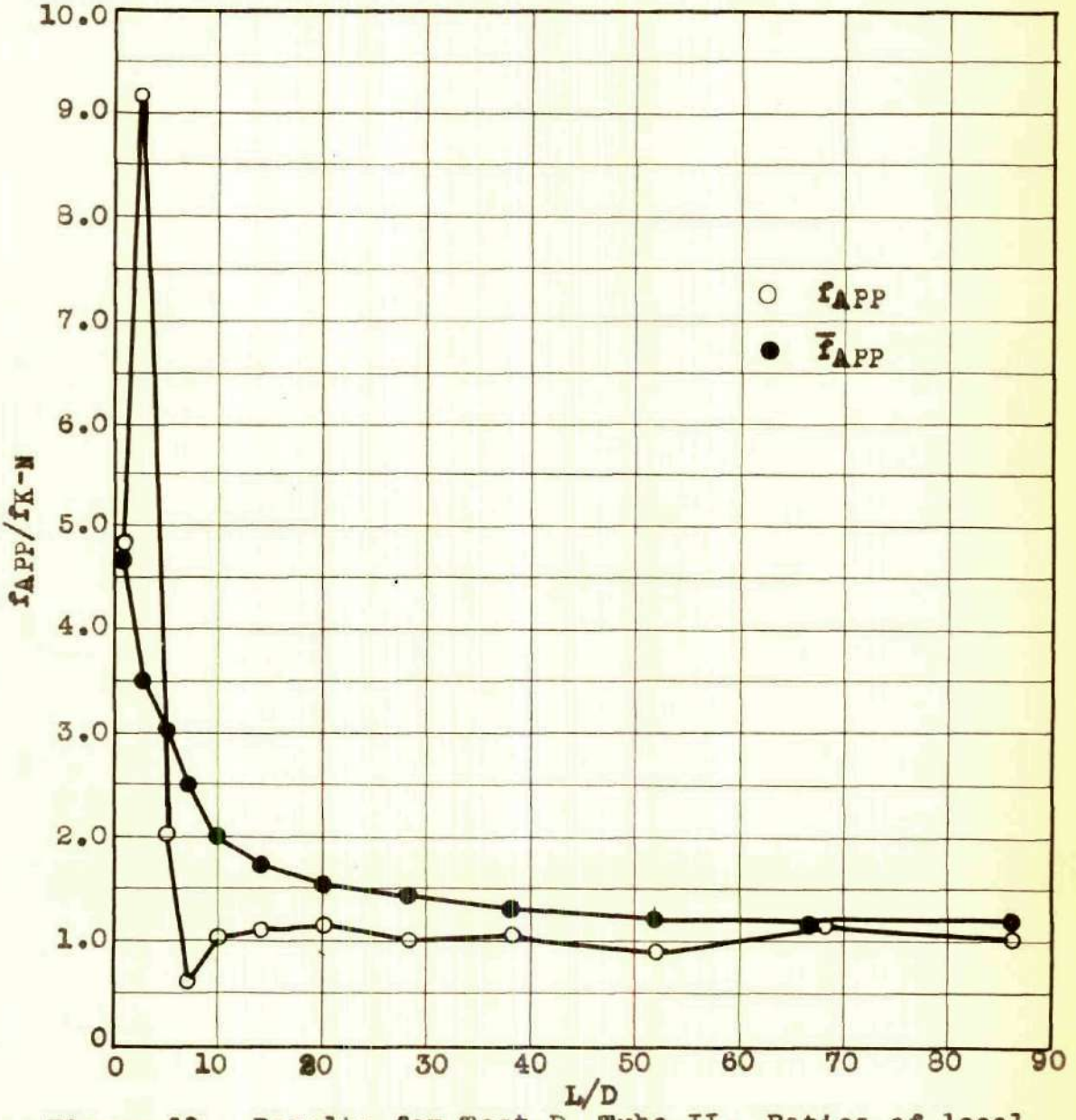

Figure 11. Results for Test D, Tube II. Ratios of local and integrated apparent friction coefficients to the Karman-Nikuradse friction coefficient against L/D for a constant value of R_D.

Table 12. Test E, Tube II.

P_{cc} = 27 psig R_D = 163,800

W_w = 266 lbs./min. f_{K-N} = 0.0163

T_w = 88° F.

Pressure Taps	ΔP ("H_2O)	f_{APP}	f_{APP}/f_{K-N}	$\overline{f}_{APP}$	$\overline{f}_{APP}/f_{K-N}$
1-2	3.30	0.0789	4.84	0.0789	4.84
2-3	+1.30	--	--	--	--
3-4	15.0	0.1792	10.98	0.0645	3.96
4-5	+8.00	--	--	--	--
5-6	5.30	0.0316	1.94	0.0557	3.42
6-7	1.60	0.0096	0.59	0.0449	2.75
7-8	6.40	0.0191	1.17	0.0354	2.17
8-9	6.20	0.0185	1.13	0.0307	1.88
9-10	13.0	0.0194	1.19	0.0272	1.67
10-11	11.0	0.0164	1.01	0.0245	1.50
11-12	19.2	0.0191	1.17	0.0227	1.39
12-13	21.2	0.0158	0.97	0.0213	1.31
13-14	24.6	0.0184	1.13	0.0203	1.24
14-15	28.2	0.0169	1.04	0.0197	1.21

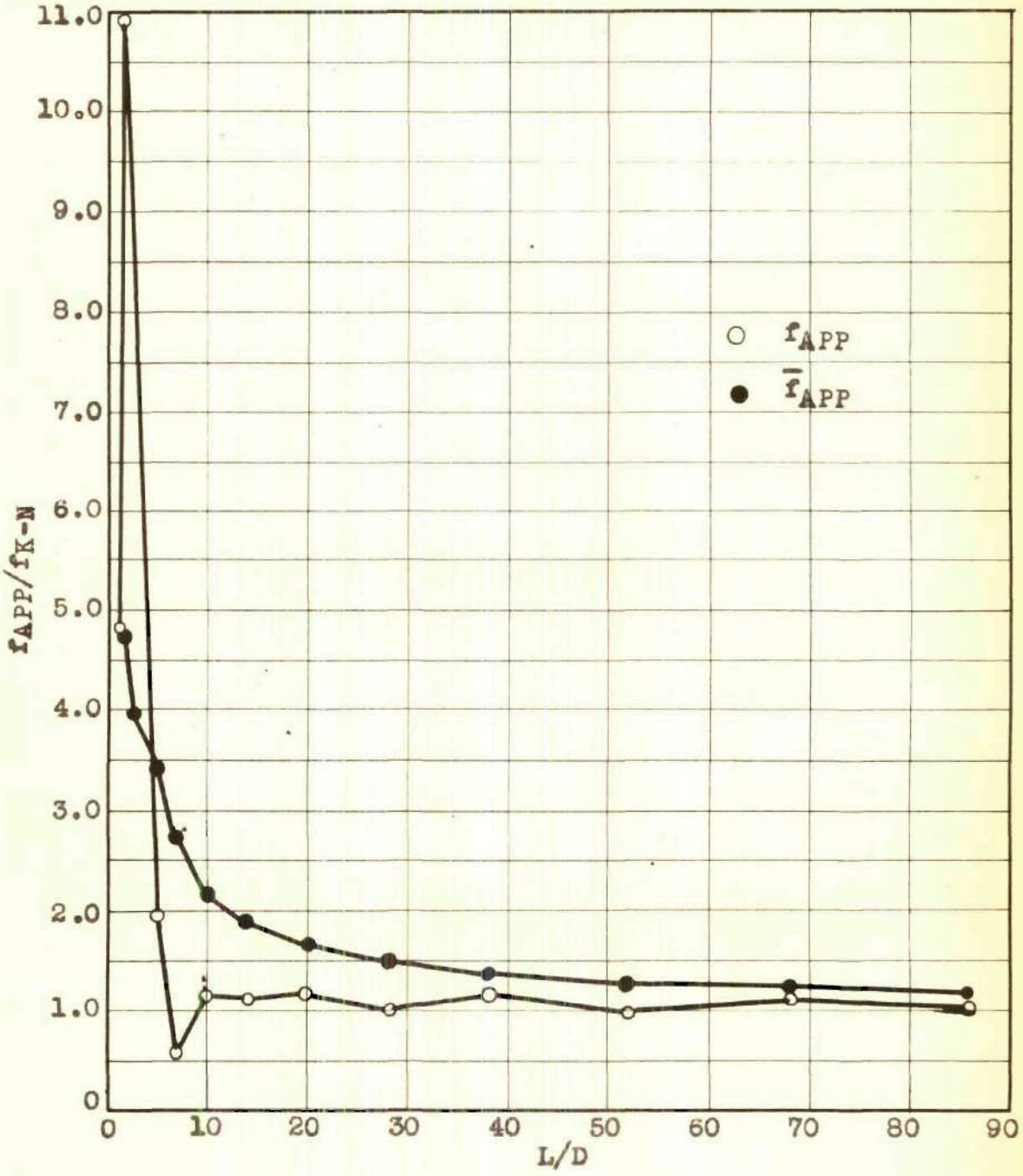

Figure 12. Results for Test E, Tube II. Ratios of local and integrated apparent friction coefficients to the Karman-Nikuradse friction coefficient against L/D for a constant value of R_D.

Table 13. Test F, Tube II.

P_{cc} = 27 psig

W_w = 330 lbs./min.

T_w = 88° F.

R_D = 203,000

f_{K-N} = 0.0156

Pressure Taps	ΔP ("H_2O)	f_{APP}	f_{APP}/f_{K-N}	$\overline{f}_{APP}$	$\overline{f}_{APP}/f_{K-N}$
1-2	5.50	0.0853	5.46	0.0853	5.46
2-3	+1.50	--	--	--	--
3-4	21.7	0.1685	10.80	0.0634	4.06
4-5	+10.4	--	--	--	--
5-6	8.00	0.0310	1.99	0.0537	3.44
6-7	1.80	0.0070	0.45	0.0430	2.76
7-8	9.20	0.0178	1.14	0.0340	2.18
8-9	9.00	0.0175	1.12	0.0291	1.86
9-10	19.6	0.0190	1.22	0.0258	1.65
10-11	15.9	0.0154	0.99	0.0233	1.49
11-12	29.0	0.0187	1.20	0.0218	1.40
12-13	30.2	0.0147	0.94	0.0203	1.30
13-14	36.8	0.0178	1.14	0.0193	1.24
14-15	40.0	0.0155	0.99	0.0188	1.20

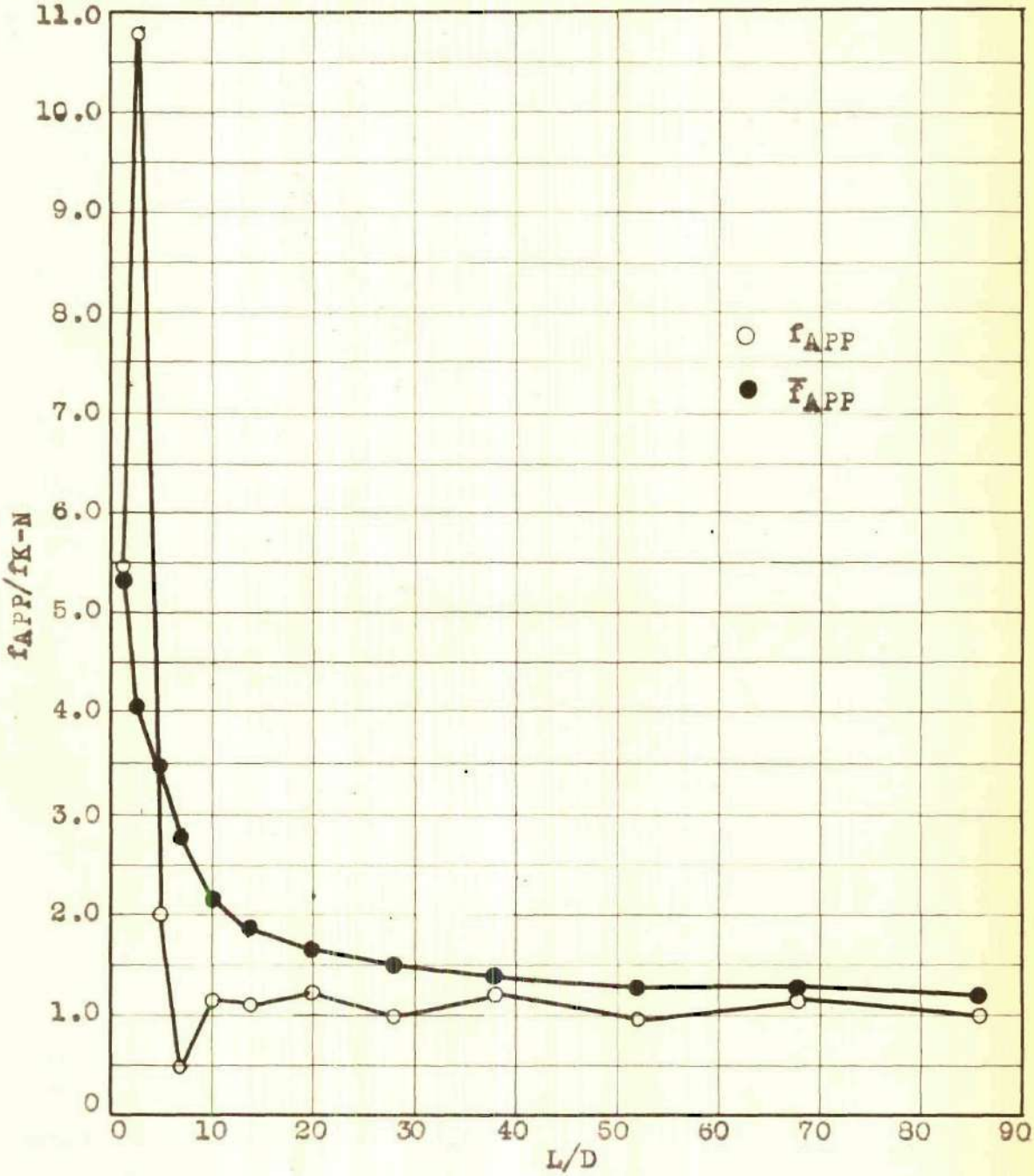

Figure 13. Results of Test F, Tube II. Ratios of local and integrated apparent friction coefficients to the Karman-Nikuradse friction coefficient against L/D for a constant value of R_D.

Table 14. Test G, Tube II.

P_{cc} = 30 psig

W_w = 425 lbs./min.

T_w = 90° F.

R_D = 267,300

f_{K-N} = 0.0148

Pressure Taps	ΔP ("H_2O)	f_{APP}	f_{APP}/f_{K-N}	$\bar{f}_{APP}$	$\bar{f}_{APP}/f_{K-N}$
1-2	12.6	0.1176	7.95	0.1176	7.95
2-3	+2.6	--	--	--	--
3-4	39.5	0.1845	12.45	0.0755	5.10
4-5	+17.0	--	--	--	--
5-6	12.0	0.0280	1.89	0.0604	4.08
6-7	2.0	0.0047	0.32	0.0467	3.15
7-8	14.0	0.0164	1.11	0.0360	2.43
8-9	14.5	0.0169	1.14	0.0302	2.04
9-10	32.0	0.0187	1.26	0.0265	1.79
10-11	25.0	0.0146	0.99	0.0236	1.59
11-12	44.7	0.0174	1.18	0.0207	1.47
12-13	49.5	0.0144	0.97	0.0200	1.35
13-14	55.5	0.0162	1.09	0.0189	1.28
14-15	67.0	0.0156	1.05	0.0183	1.24

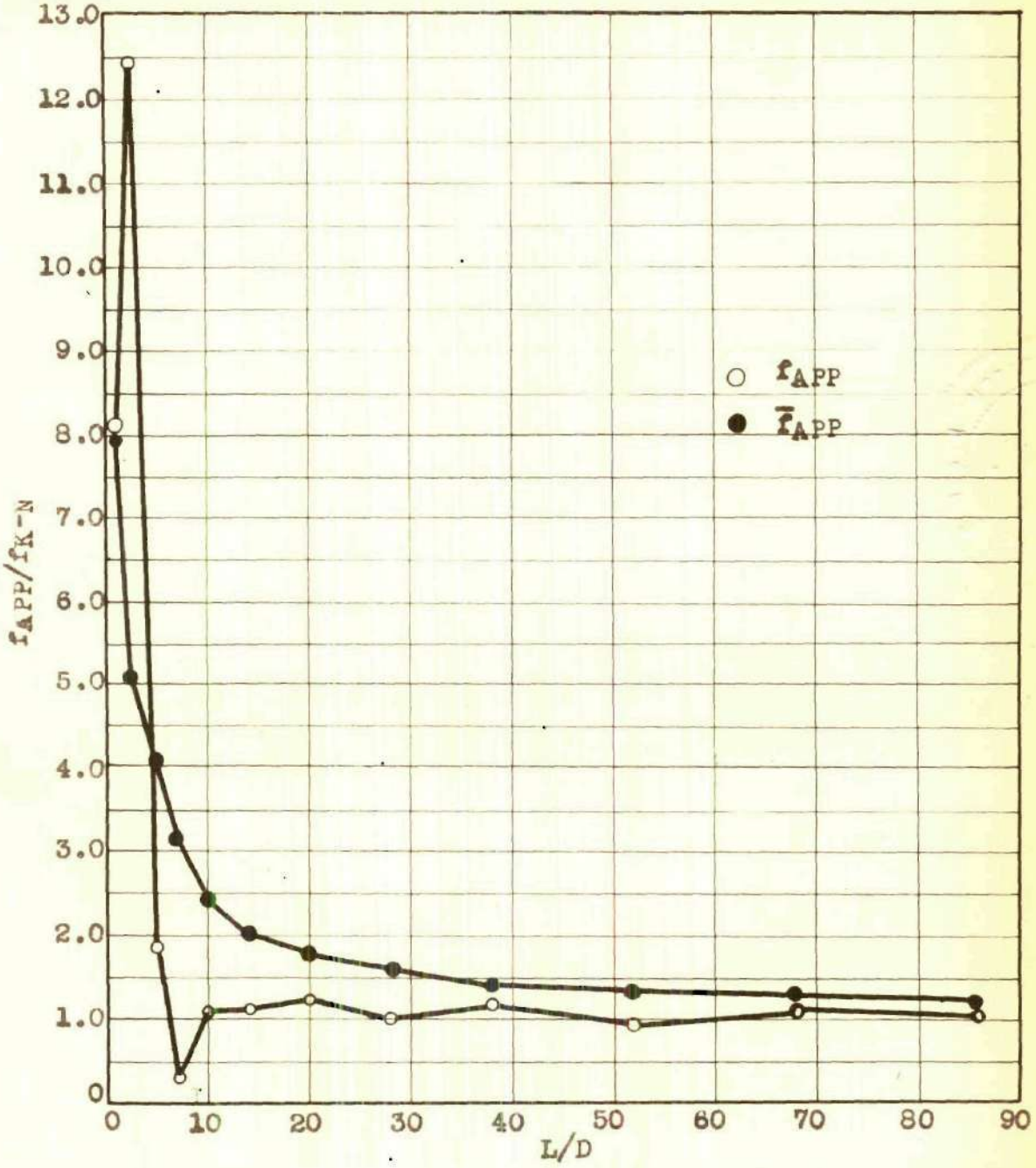

Figure 14. Results for Test G, Tube II. Ratios of local and integrated apparent friction coefficients to the Karman-Nikuradse friction coefficient against L/D for a constant value of R_D.

Table 15. Test H, Tube II.

P_{cc} = 44 psig R_D = 330,000

W_w = 525 lbs./min. f_{K-N} = 0.0142

T_w = 90° F.

Pressure Taps	ΔP ("H_2O)	f_{APP}	f_{APP}/f_{K-N}	$\bar{f}_{APP}$	$\bar{f}_{APP}/f_{K-N}$
1-2	20.4	0.1250	8.80	0.1250	8.80
2-3	3.4	--	--	--	--
3-4	54.2	0.1660	11.70	0.0778	5.48
4-5	+28.4	--	--	--	--
5-6	17.6	0.0269	1.89	0.0590	4.15
6-7	3.4	0.0052	0.37	0.0458	3.22
7-8	21.0	0.0161	1.13	0.0353	2.48
8-9	20.3	0.0155	1.09	0.0295	2.08
9-10	50.1	0.0191	1.35	0.0260	1.83
10-11	39.3	0.0150	1.06	0.0234	1.65
11-12	67.8	0.0173	1.22	0.0215	1.51
12-13	76.0	0.0145	1.02	0.0199	0.40
13-14	86.7	0.0166	1.17	0.0189	1:33
14-15	109.0	0.0167	1.17	0.0184	1:29

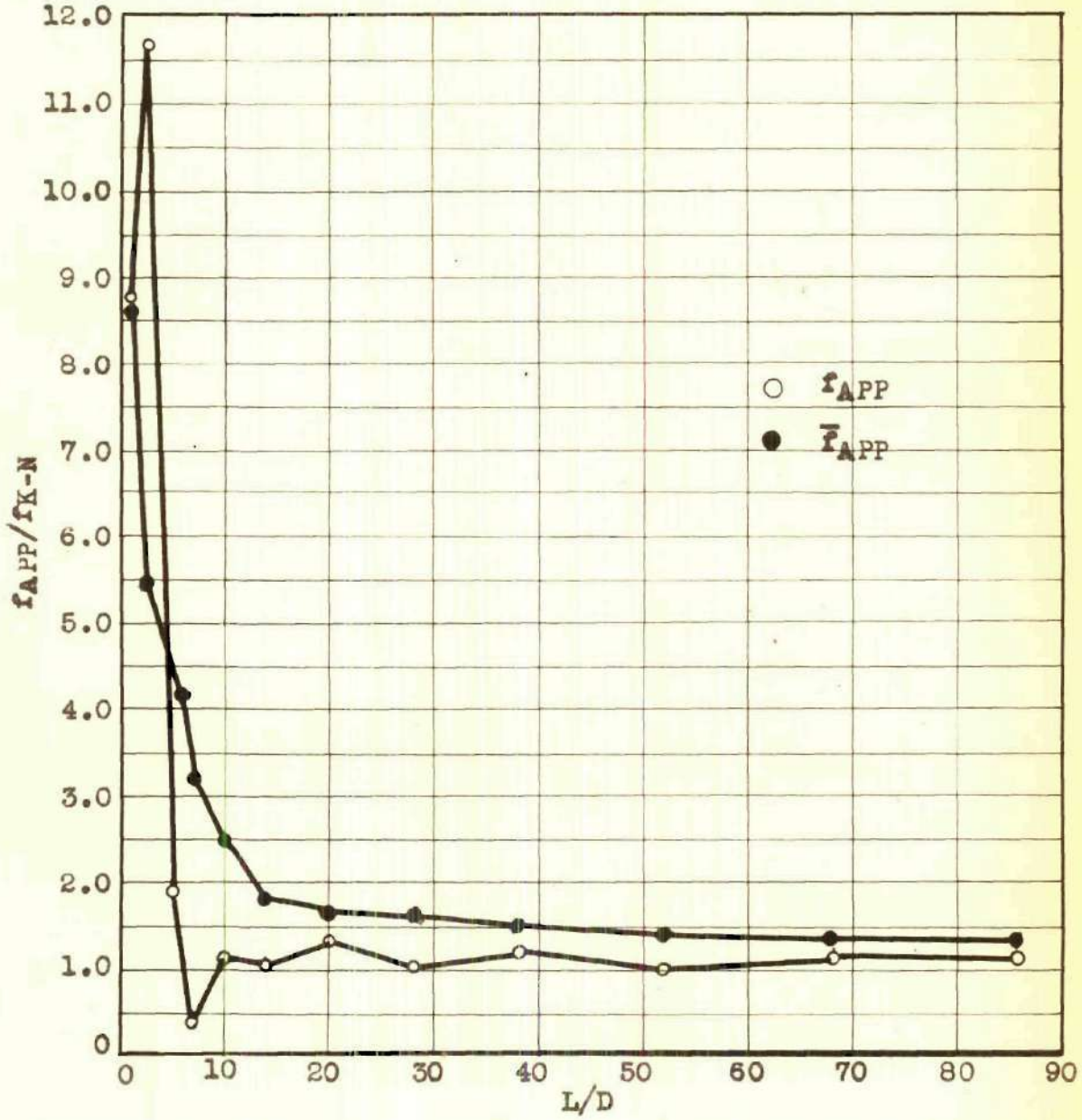

Figure 15. Results for Test H, Tube II. Ratios of local and integrated apparent friction coefficients to the Karman-Nikuradse friction coefficient against L/D for a constant value of R_D.

Table 16. Test A, Tube III.

P_{cc} = 24 psig

W_w = 51 lbs./min.

T_w = 90° F.

R_D = 46,300

f_{K-N} = 0.0212

Pressure Taps	ΔP ("H_2O)	f_{APP}	f_{APP}/f_{K-N}	$\overline{f}_{APP}$	$\overline{f}_{APP}/f_{K-N}$
1-2	0.40	0.0301	1.42	0.0301	1.42
2-3	0.14	0.0211	1.00	0.0283	1.34
3-4	0.14	0.0105	0.49	0.0229	1.08
4-5	0.30	0.0226	1.07	0.0208	0.98
5-6	0.36	0.0135	0.64	0.0194	0.92
6-7	0.40	0.0150	0.71	0.0178	0.84
7-8	0.96	0.0181	0.85	0.0176	0.83
8-9	0.94	0.0177	0.83	0.0177	0.84
9-10	3.84	0.0361	1.70	0.0214	1.01
10-11	1.52	0.0143	0.68	0.0225	1.06
11-12	6.20	0.0389	1.83	0.0242	1.14
12-13	3.00	0.0142	0.67	0.0244	1.15
13-14	3.70	0.0174	0.82	0.0224	1.06
14-15	7.30	0.0275	1.29	0.0225	1.06

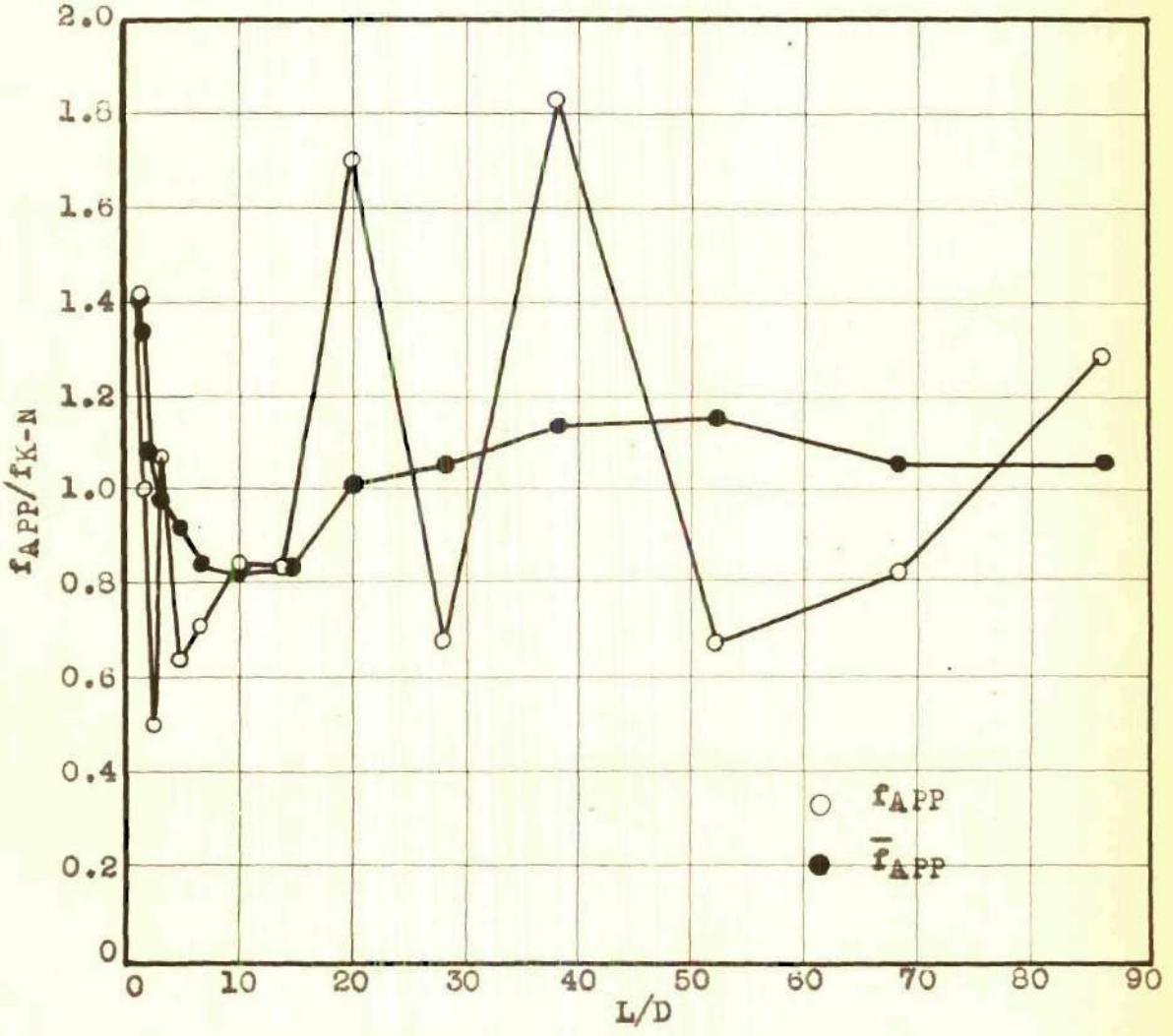

Figure 16. Results for Test A, Tube III. Ratios of local and integrated apparent friction coefficients to the Karman-Nikuradse friction coefficient against L/D for a constant value of R_D.

Table 17. Test B, Tube III.

P_{cc} = 26 psig

W_w = 91 lbs./min.

T_w = 89° F.

R_D = 81,700

f_{K-N} = 0.0188

Pressure Taps	ΔP ("H_2O)	f_{APP}	f_{APP}/f_{K-N}	$\bar{f}_{APP}$	$\bar{f}_{APP}/f_{K-N}$
1-2	0.84	0.0197	1.05	0.0197	1.05
2-3	0.20	0.0094	0.50	0.0177	0.94
3-4	0.48	0.0113	0.60	0.0150	0.80
4-5	0.86	0.0202	1.07	0.0153	0.81
5-6	0.84	0.0098	0.52	0.0146	0.78
6-7	1.00	0.0118	0.63	0.0135	0.72
7-8	4.90	0.0288	1.53	0.0165	0.88
8-9	3.20	0.0188	1.00	0.0187	0.99
9-10	12.0	0.0352	1.87	0.0221	1.18
10-11	3.20	0.0094	0.50	0.0221	1.18
11-12	17.6	0.0346	1.84	0.0228	1.21
12-13	8.00.	0.0118	0.63	0.0224	1.19
13-14	8.70	0.0128	0.68	0.0200	1.06
14-15	20.5	0.0241	1.28	0.0198	1.05

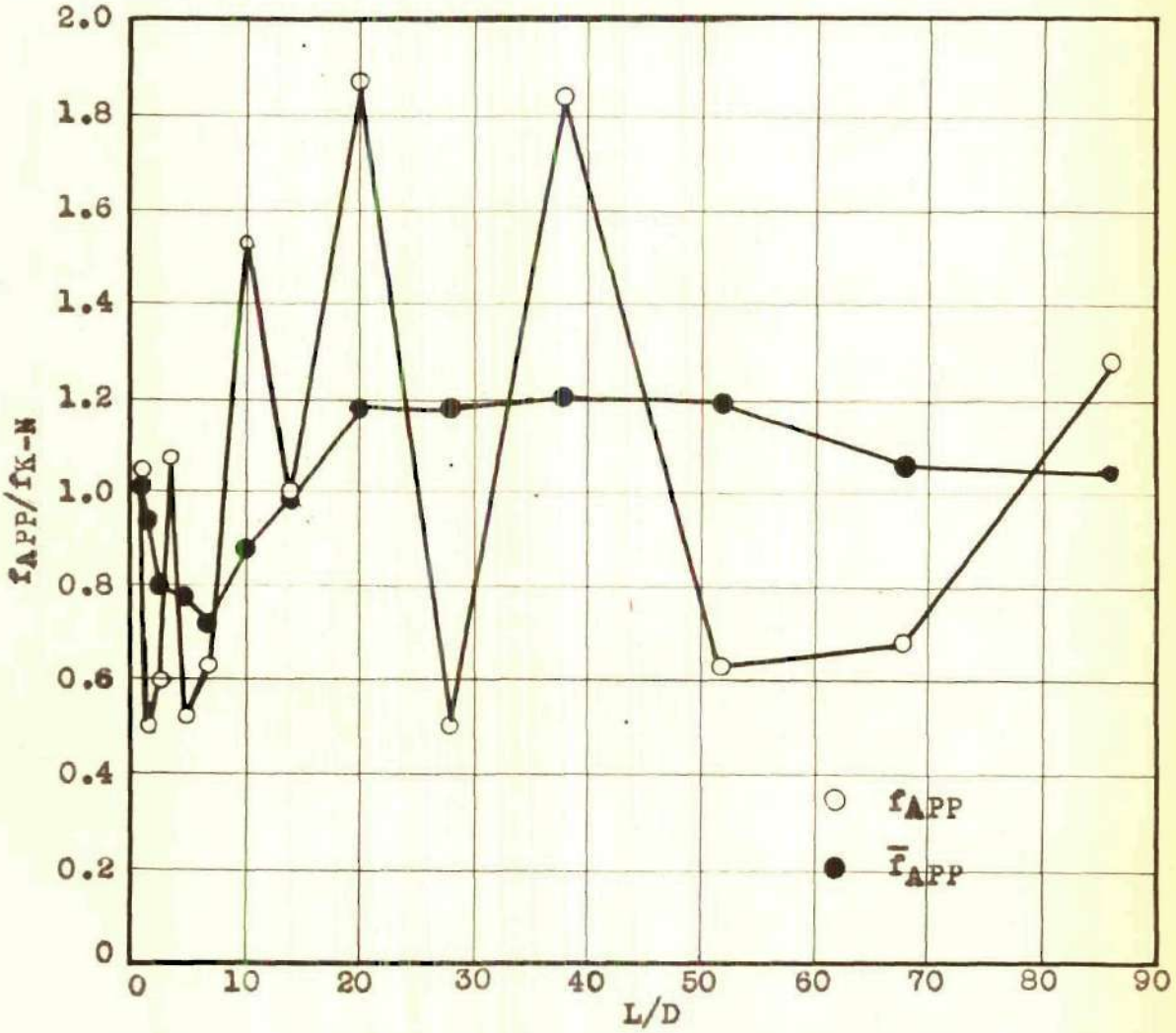

Figure 17. Results for Test B, Tube III. Ratios of local and integrated apparent friction coefficients to the Karman-Nikuradse friction coefficient against L/D for a constant value of R_D.

Table 18. Test C, Tube III.

P_{cc} = 27 psig

W_w = 119 lbs./min.

T_w = 89° F.

R_D = 106,800

f_{K-N} = 0.0178

Pressure Taps	ΔP ("H_2O)	f_{APP}	f_{APP}/f_{K-N}	$\bar{f}_{APP}$	$\bar{f}_{APP}/f_{K-N}$
1-2	1.46	0.0201	1.13	0.0201	1.13
2-3	0.36	0.0099	0.56	0.0180	1.01
3-4	0.54	0.0074	0.42	0.0144	0.81
4-5	2.04	0.0280	1.58	0.0155	0.87
5-6	1.10	0.0076	0.43	0.0151	0.85
6-7	1.96	0.0135	0.76	0.0137	0.77
7-8	8.20	0.0282	1.59	0.0167	0.94
8-9	5.10	0.0175	0.99	0.0185	1.04
9-10	18.2	0.0313	1.76	0.0211	1.19
10-11	5.00	0.0086	0.48	0.0207	1.17
11-12	29.0	0.0332	1.87	0.0214	1.21
12-13	12.7	0.0109	0.61	0.0212	1.20
13-14	14.8	0.0127	0.72	0.0190	1.07
14-15	32.0	0.0220	1.24	0.0188	1.06

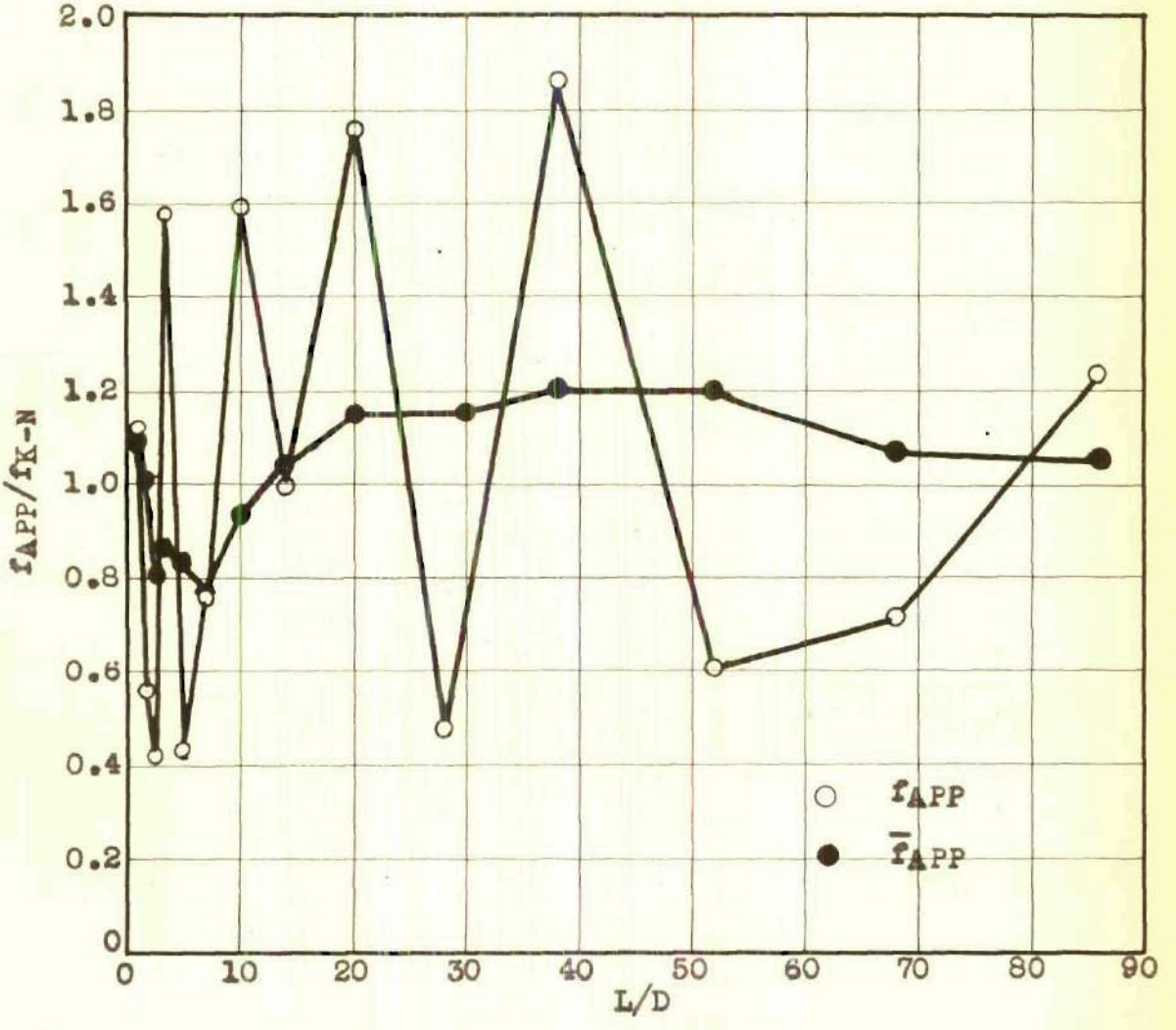

Figure 18. Results for Test C, Tube III. Ratios of local and integrated apparent friction coefficients to the Karman-Nikuradse friction coefficient against L/D for a constant value of R_D.

Table 19. Test D, Tube III.

P_{cc} = 26 psig R_D = 132,000

W_w = 147 lbs./min. f_{K-N} = 0.0170

T_w = 89° F.

Pressure Taps	ΔP ("H_2O)	f_{APP}	f_{APP}/f_{K-N}	$\overline{f}_{APP}$	$\overline{f}_{APP}/f_{K-N}$
1-2	2.60	0.0234	1.38	0.0234	1.38
2-3	0.50	0.0090	0.53	0.0205	1.20
3-4	0.80	0.0072	0.42	0.0157	0.92
4-5	2.80	0.0252	1.48	0.0159	0.93
5-6	2.00	0.0090	0.53	0.0154	0.91
6-7	4.00	0.0180	1.06	0.0148	0.87
7-8	13.4	0.0302	1.78	0.0184	1.08
8-9	8.10	0.0182	1.07	0.0201	1.18
9-10	29.0	0.0326	1.92	0.0225	1.32
10-11	5.60	0.0063	0.37	0.0216	1.27
11-12	40.6	0.0305	1.79	0.0214	1.26
12-13	17.6	0.0099	0.58	0.0207	1.22
13-14	22.4	0.0126	0.74	0.0184	1.08
14-15	49.5	0.0223	1.31	0.0183	1.07

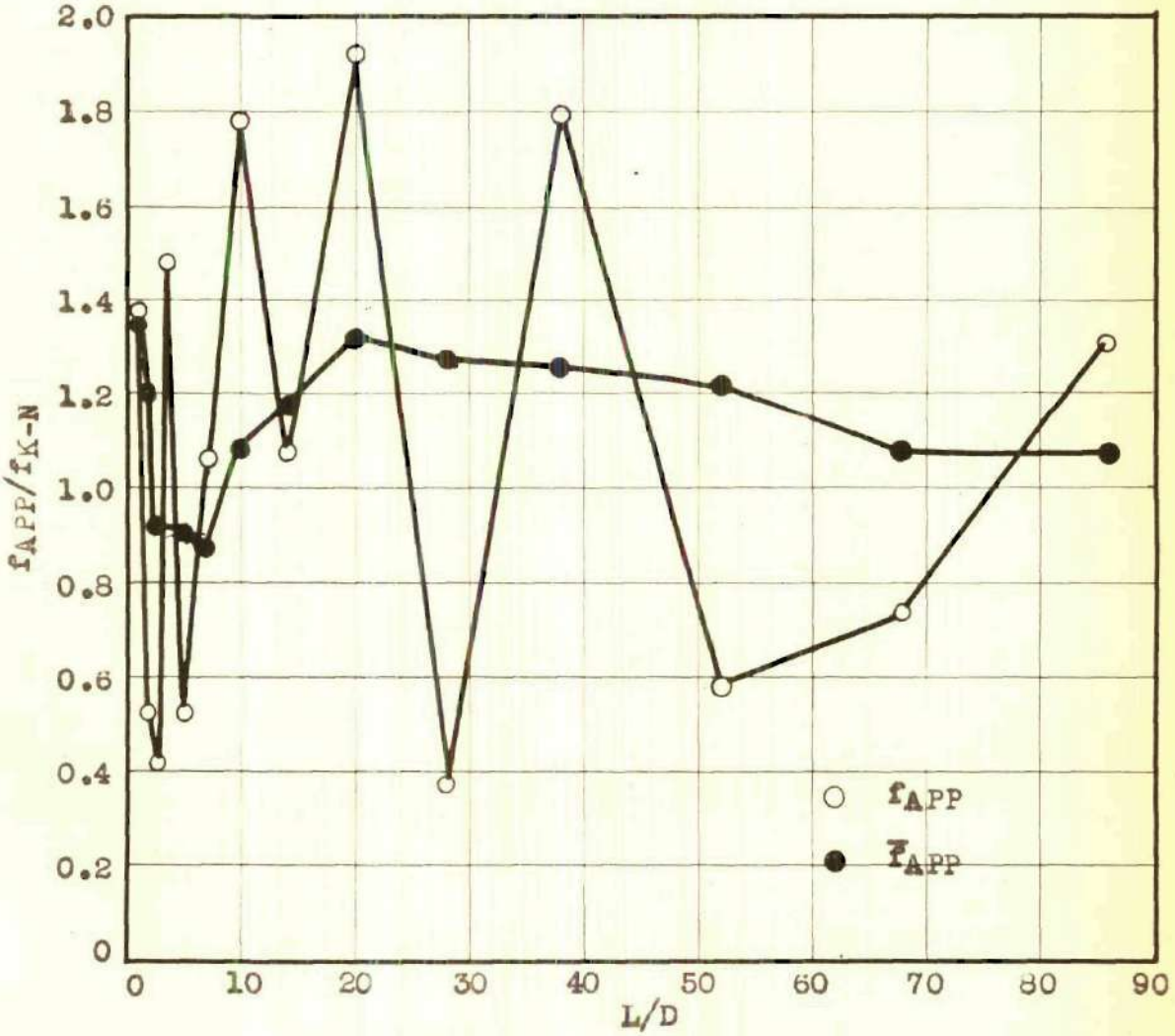

Figure 19. Results for Test D, Tube III. Ratios of local and integrated apparent friction coefficients to the Karman—Nikuradse friction coefficient against L/D for a constant value of R_D.

Table 20. Test E, Tube III.

P_{cc} = 29 psig

W_w = 170 lbs./min.

T_w = 90° F.

R_D = 154,200

f_{K-N} = 0.0165

Pressure Taps	ΔP ("H_2O)	f_{APP}	f_{APP}/f_{K-N}	$\overline{f}_{APP}$	$\overline{f}_{APP}/f_{K-N}$
1-2	3.40	0.0229	1.39	0.0229	1.39
2-3	0.70	0.0095	0.58	0.0202	1.22
3-4	0.50	0.0034	0.21	0.0147	0.89
4-5	3.50	0.0236	1.43	0.0143	0.87
5-6	3.10	0.0105	0.64	0.0145	0.88
6-7	5.40	0.0182	1.10	0.0144	0.87
7-8	16.5	0.0278	1.69	0.0177	1.07
8-9	9.00	0.0152	0.92	0.0188	1.14
9-10	36.0	0.0304	1.84	0.0208	1.26
10-11	6.00	0.0051	0.31	0.0199	1.20
11-12	52.0	0.0292	1.77	0.0198	1.20
12-13	23.7	0.0100	0.61	0.0194	1.18
13-14	27.8	0.0117	0.71	0.0174	1.05
14-15	65.0	0.0219	1.33	0.0174	1.05

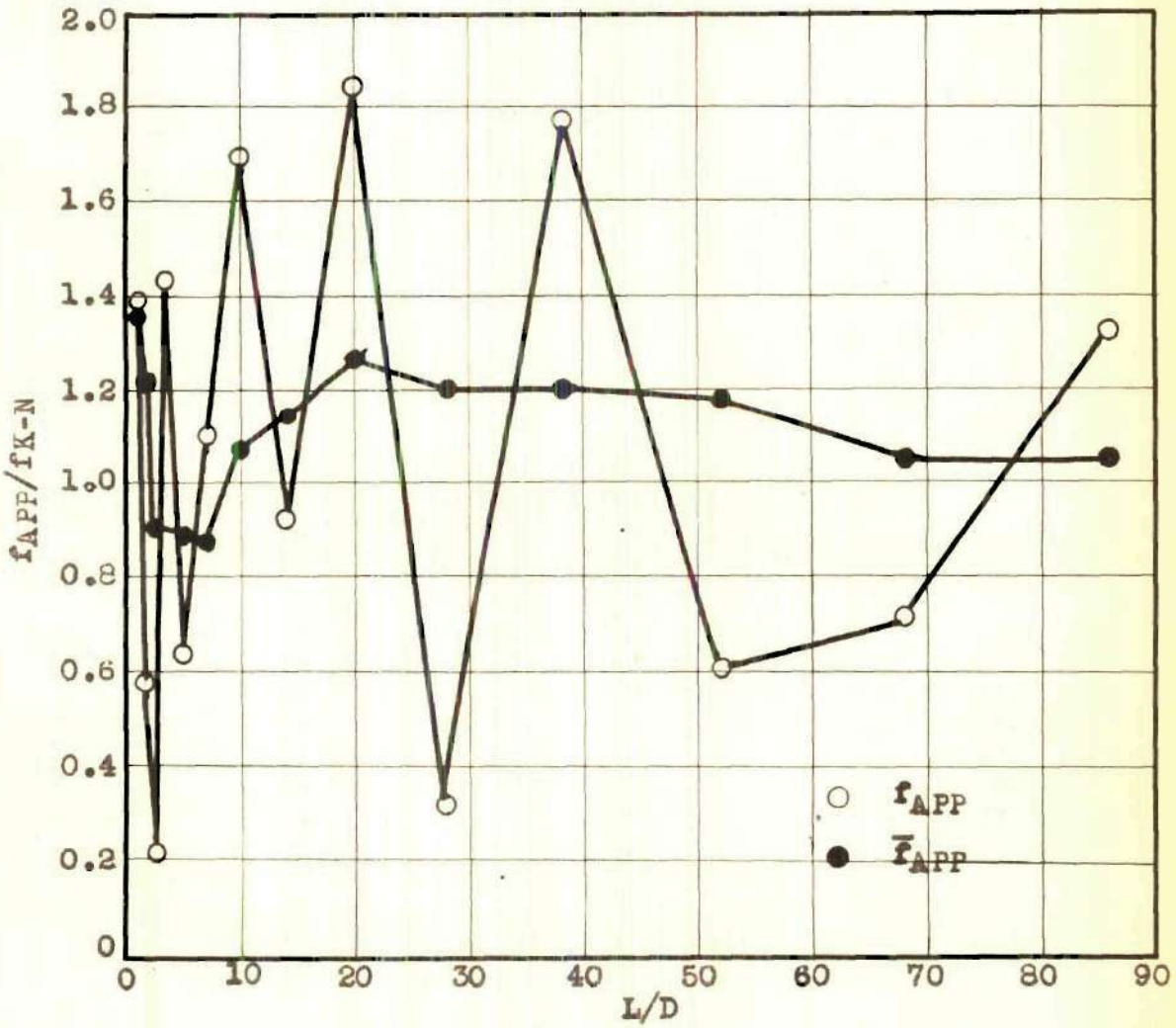

Figure 20. Results for Test E, Tube III. Ratios of local and integrated apparent friction coefficients to the Karman-Nikuradse friction coefficient against L/D for a constant value of R_D.

Table 21. Test F, Tube III.

P_{cc} = 38 psig

W_w = 217 lbs./min.

T_w = 90° F.

R_D = 197,000

f_{K-N} = 0.0157

Pressure Taps	ΔP ("H_2O)	f_{APP}	f_{APP}/f_{K-N}	$\overline{f}_{APP}$	$\overline{f}_{APP}/f_{K-N}$
1-2	6.40	0.0265	1.69	0.0215	1.69
2-3	1.10	0.0091	0.58	0.0231	1.47
3-4	0.70	0.0039	0.25	0.0163	1.04
4-5	5.10	0.0212	1.35	0.0149	0.95
5-6	10.0	0.0207	1.32	0.0169	1.08
6-7	9.00	0.0187	1.19	0.0178	1.13
7-8	29.0	0.0310	1.92	0.0204	1.30
8-9	14.8	0.0154	0.98	0.0211	1.34
9-10	57.0	0.0296	1.88	0.0222	1.41
10-11	7.45	0.0039	0.25	0.0206	1.31
11-12	88.0	0.0304	1.93	0.0204	1.30
12-13	38.0	0.0099	0.63	0.0200	1.27
13-14	40.7	0.0105	0.67	0.0176	1.12
14-15	100.5	0.0208	1.32	0.0174	1.11

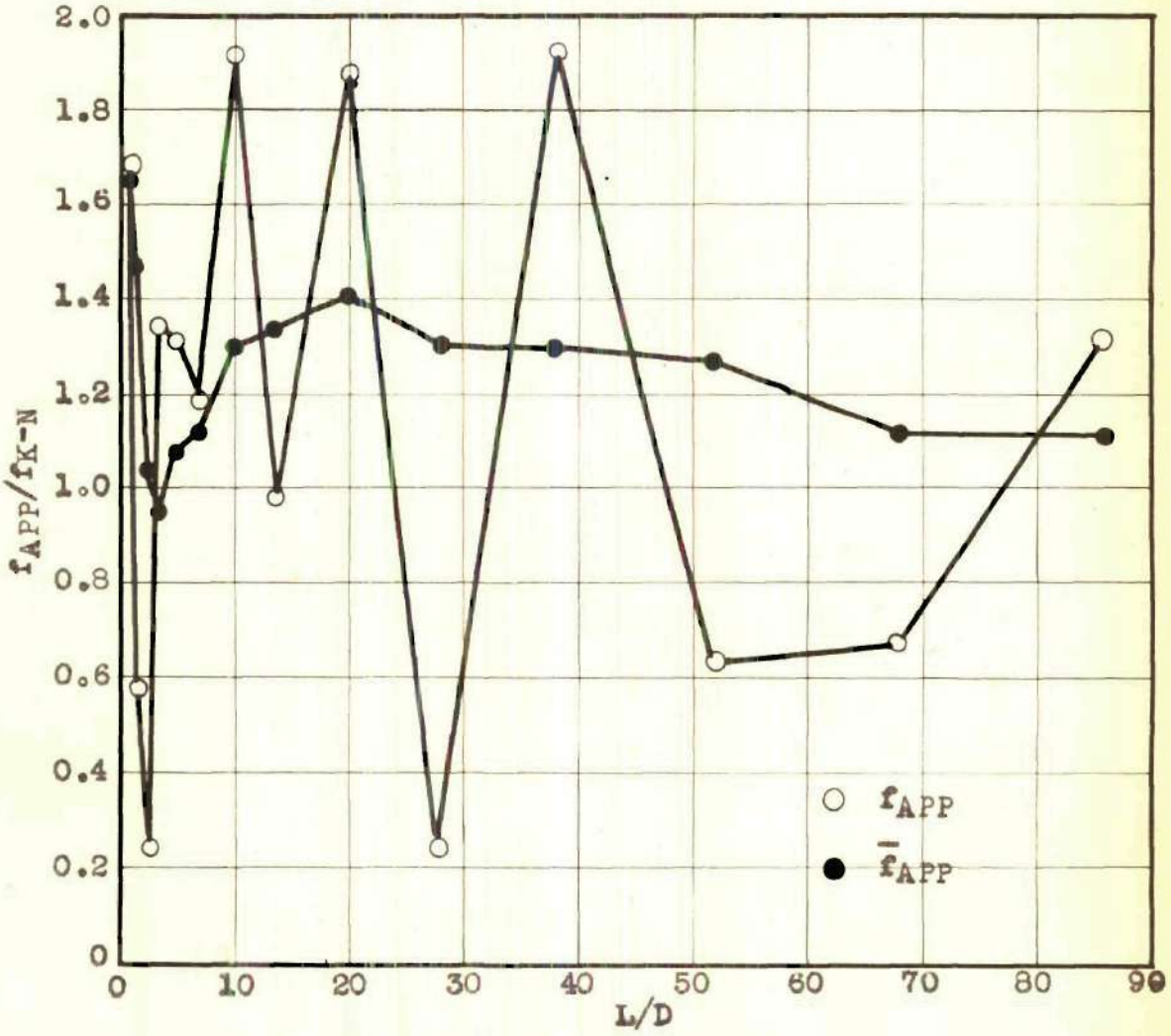

Figure 21. Results for Test F, Tube III. Ratios of local and integrated apparent friction coefficients to the Karman-Nikuradse friction coefficient against L/D for a constant value of R_D.

Table 22. Test G, Tube III.

P_{cc} = 55 psig

W_w = 268 lbs./min.

T_w = 89° F.

R_D = 241,000

f_{K-N} = 0.0151

Pressure Taps	ΔP ("H_2O)	f_{APP}	f_{APP}/f_{K-N}	$\bar{f}_{APP}$	$\bar{f}_{APP}/f_{K-N}$
1-2	7.80	0.0211	1.40	0.0211	1.40
2-3	2.20	0.0119	0.79	0.0193	1.28
3-4	1.50	0.0041	0.27	0.0146	0.97
4-5	8.70	0.0236	1.56	0.0143	0.95
5-6	15.5	0.0210	1.39	0.0168	1.11
6-7	12.8	0.0174	1.15	0.0176	1.16
7-8	44.0	0.0298	1.97	0.0201	1.33
8-9	25.1	0.0170	1.13	0.0211	1.40
9-10	102.0	0.0346	2.29	0.0234	1.55
10-11	1.40	0.0011	0.07	0.0207	1.44
11-12	154.5	0.0349	2.31	0.0216	1.43
12-13	42.0	0.0071	0.47	0.0209	1.38
13-14	44.0	0.0075	0.50	0.0176	1.16
14-15	158.0	0.0214	1.42	0.0172	1.14

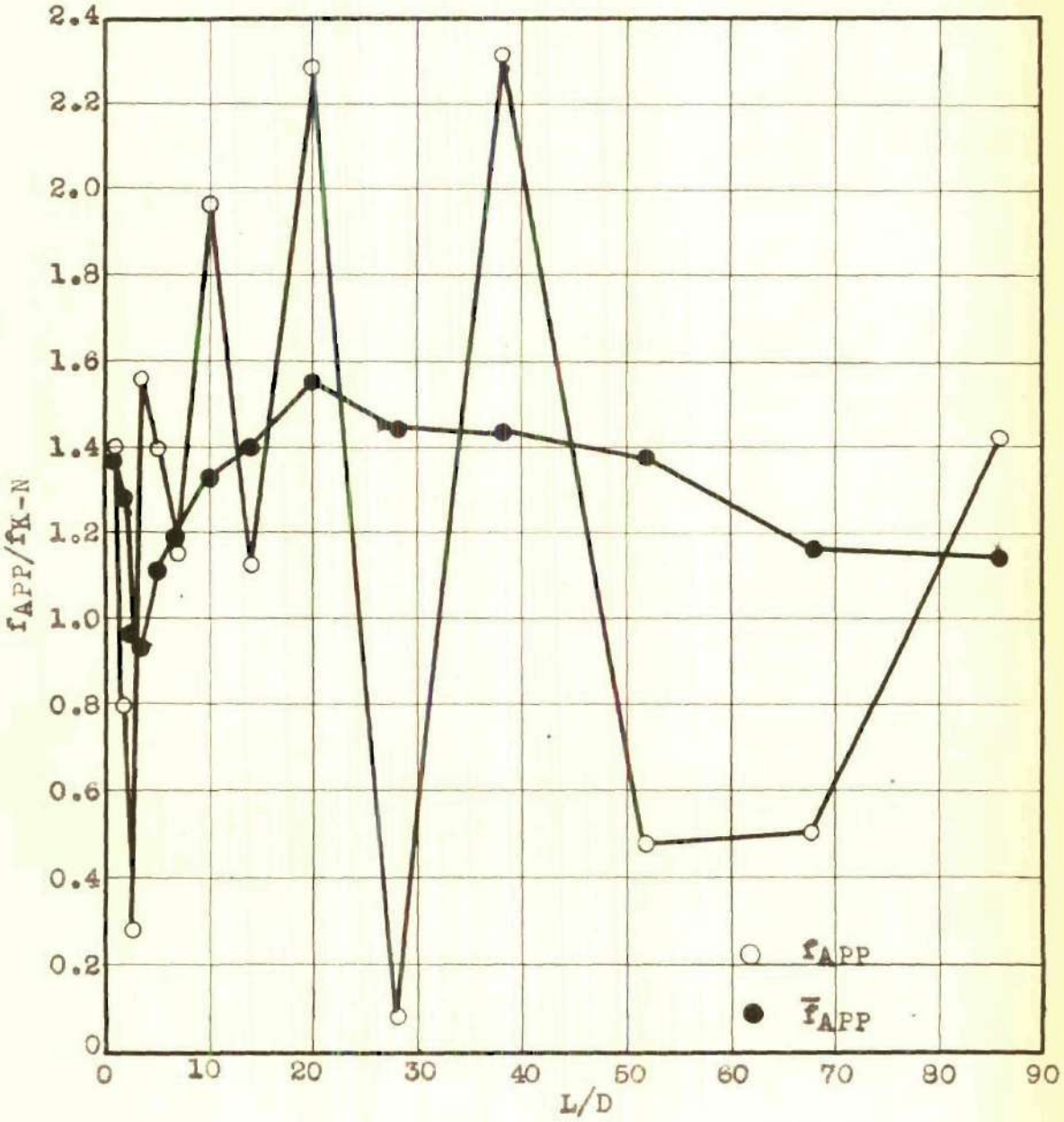

Figure 22. Results for Test G, Tube III. Ratios of local and integrated apparent friction coefficient to the Karman-Nikuradse friction coefficient against L/D for a constant value of R_D.

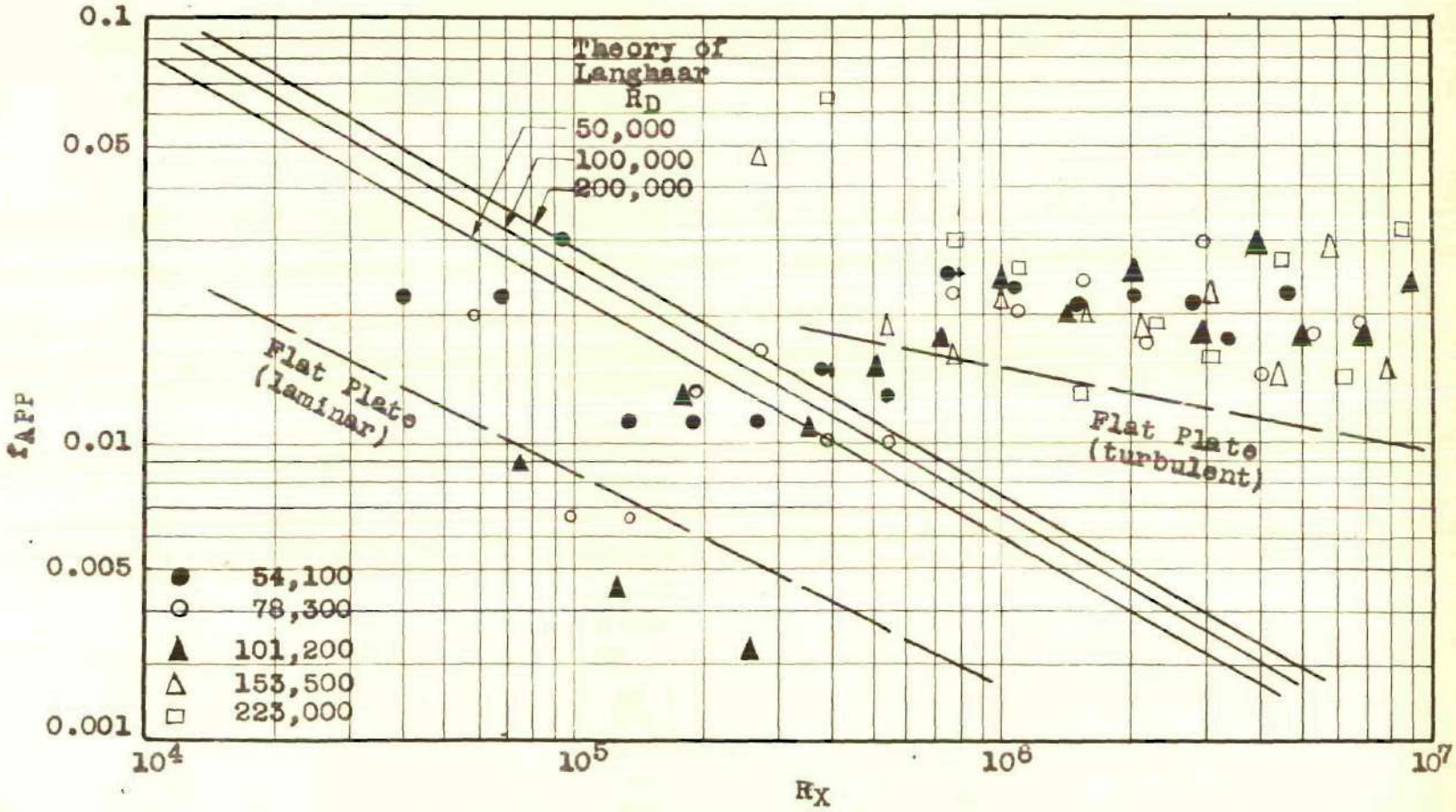

Figure 23. Results of Tube I. Value of f_{APP} against R_X for constant values of R_D. Comparison with flat plate theory and laminar flow theory of Langhaar.

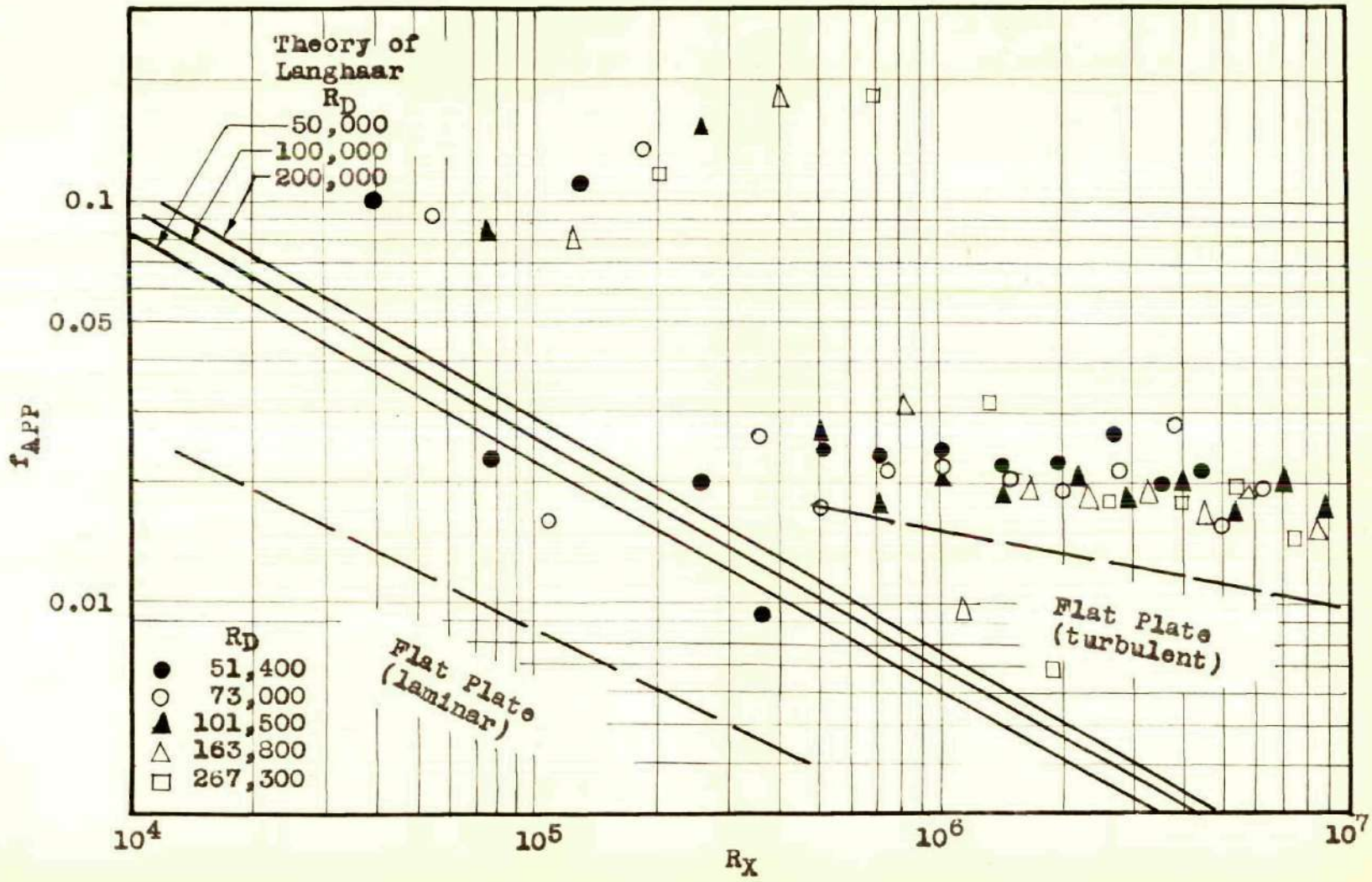

Figure 24. Results for Tube II. Value of f_{APP} against R_X for constant values of R_D. Comparison with flat plate theory and laminar flow theory of Langhaar.

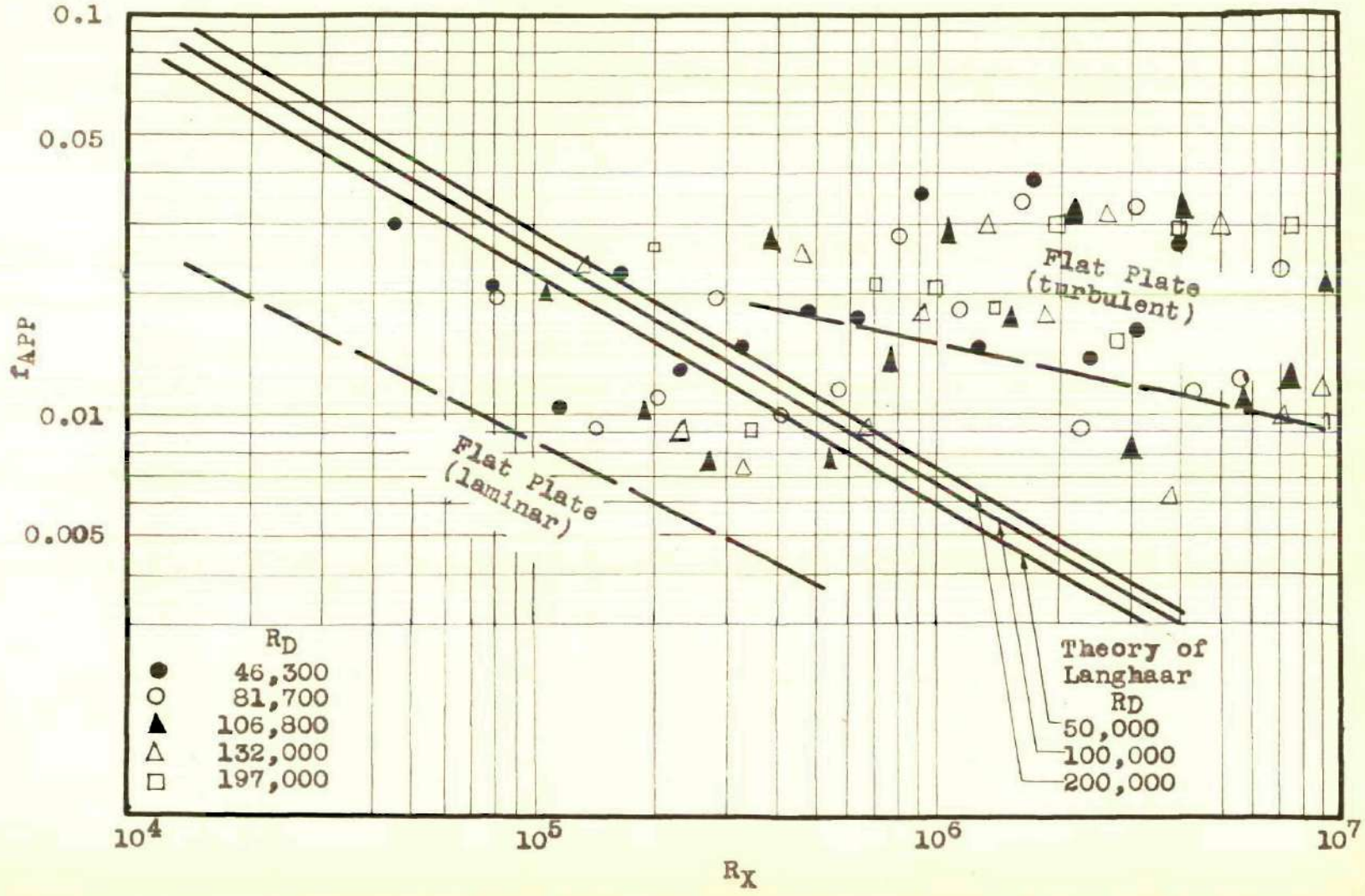

Figure 25. Results for Tube III. Value of f_{APP} against R_X for constant values of R_D. Comparison with flat plate theory and laminar flow theory of Langhaar.

APPENDIX B

METHODS OF CALCULATION

METHODS OF CALCULATION

The Reynolds number based on tube diameter is defined by

$$R_D = VD\rho/\mu$$

where V is the mean velocity in respect to the mass rate of flow and the density ρ and viscosity μ are evaluated at the mean temperature and pressure of the stream.

The Reynolds number based on distance from the inlet is defined by

$$R_X = VX\rho/\mu$$

where X is the axial distance from the inlet to the point concerned.

The local apparent friction coefficient is defined by

$$p_1 - p_2 = f_{APP} \frac{X_2 - X_1}{D} \frac{V^2}{2g}$$

where p_1 and p_2 are the static pressures, measured at the tube wall, at the axial locations X_1 and X_2 respectively. The value of f_{APP} calculated was taken to be the local value midway between X_1 and X_2. The velocity V is the mean value based on the mass rate of flow.

The integrated apparent friction coefficient at any point X is defined by

$$p_0 - p = \bar{f}_{APP} \frac{X - X_0}{D} \frac{V^2}{2g}$$

where p_0 and p are the static pressures measured at the first pressure tap and point X respectively.

The Karman-Nikuradse coefficient is defined by the relationship

$$\frac{1}{f_{K-N}} = 2.0 \log_{10} (R_D f_{K-N}) - 0.8.$$

APPENDIX C

APPARATUS

Table 23. Location and Size of Pressure Taps.

	Tube I		Tube II		Tube III	
	D = 1.028		D = 0.785		D = 0.545	
Tap	X/D	d	X/D	d	X/D	d
1	0.50	0.0260	0.50	0.0225	0.50	0.0225
2	1.00	0.0260	1.00	0.0225	1.50	0.0225
3	1.50	0.0260	2.00	0.0225	2.00	0.0225
4	2.00	0.0260	3.00	0.0225	3.00	0.0225
5	3.00	0.0260	4.00	0.0260	4.00	0.0225
6	4.00	0.0260	6.00	0.0260	6.00	0.0225
7	6.00	0.0260	8.00	0.0260	8.00	0.0225
8	8.00	0.0260	12.0	0.0260	12.0	0.0225
9	12.0	0.0260	16.0	0.0260	16.0	0.0225
10	16.0	0.0260	24.0	0.0260	24.0	0.0225
11	24.0	0.0260	32.0	0.0260	32.0	0.0225
12	32.0	0.0260	44.0	0.0260	44.0	0.0225
13	44.0	0.0260	60.0	0.0260	60.0	0.0225
14	60.0	0.0260	76.0	0.0260	76.0	0.0225
15	76.0	0.0260	96.0	0.0260	96.0	0.0225
16	96.0	0.0260				

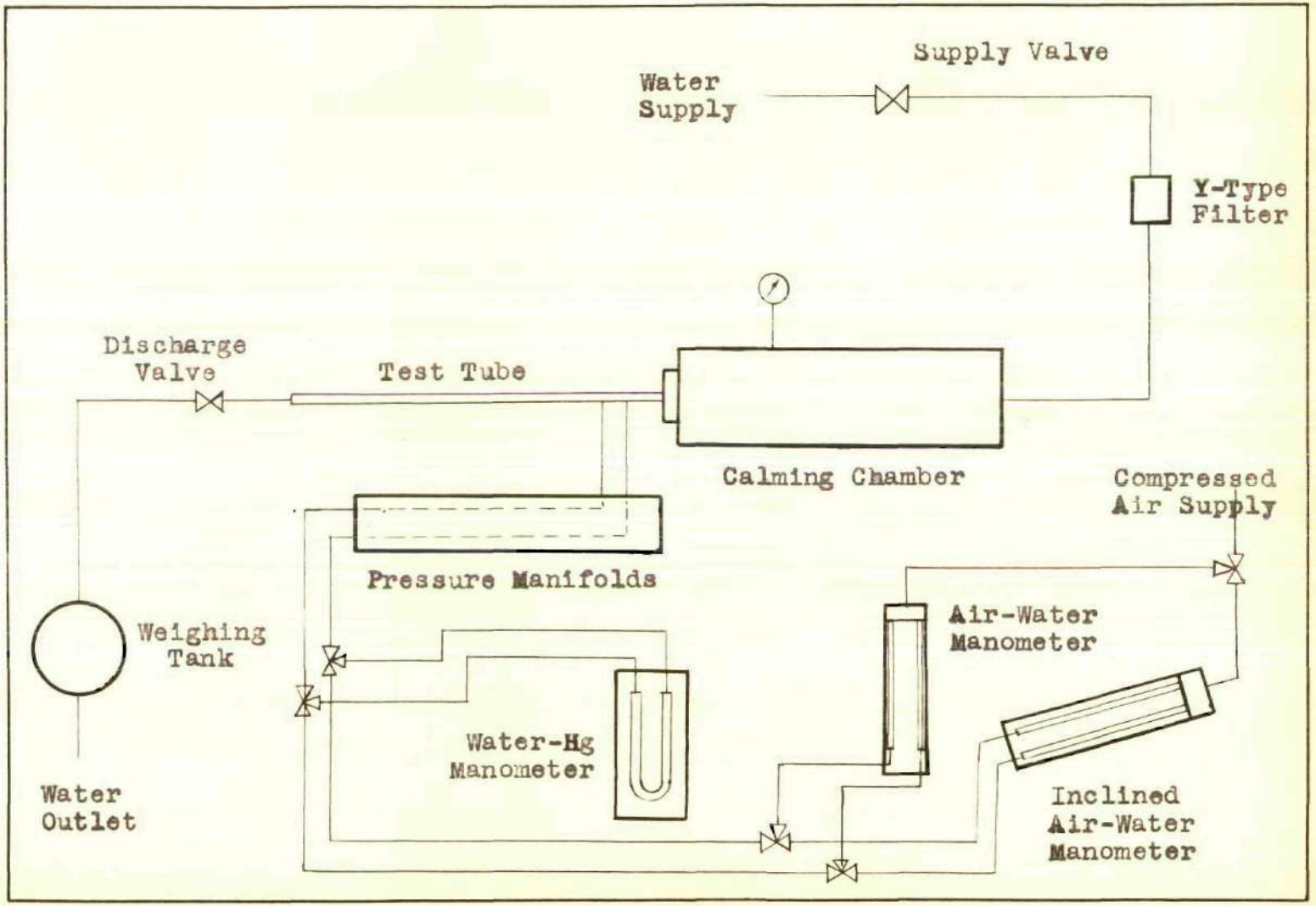

Figure 26. Flow Diagram of Apparatus

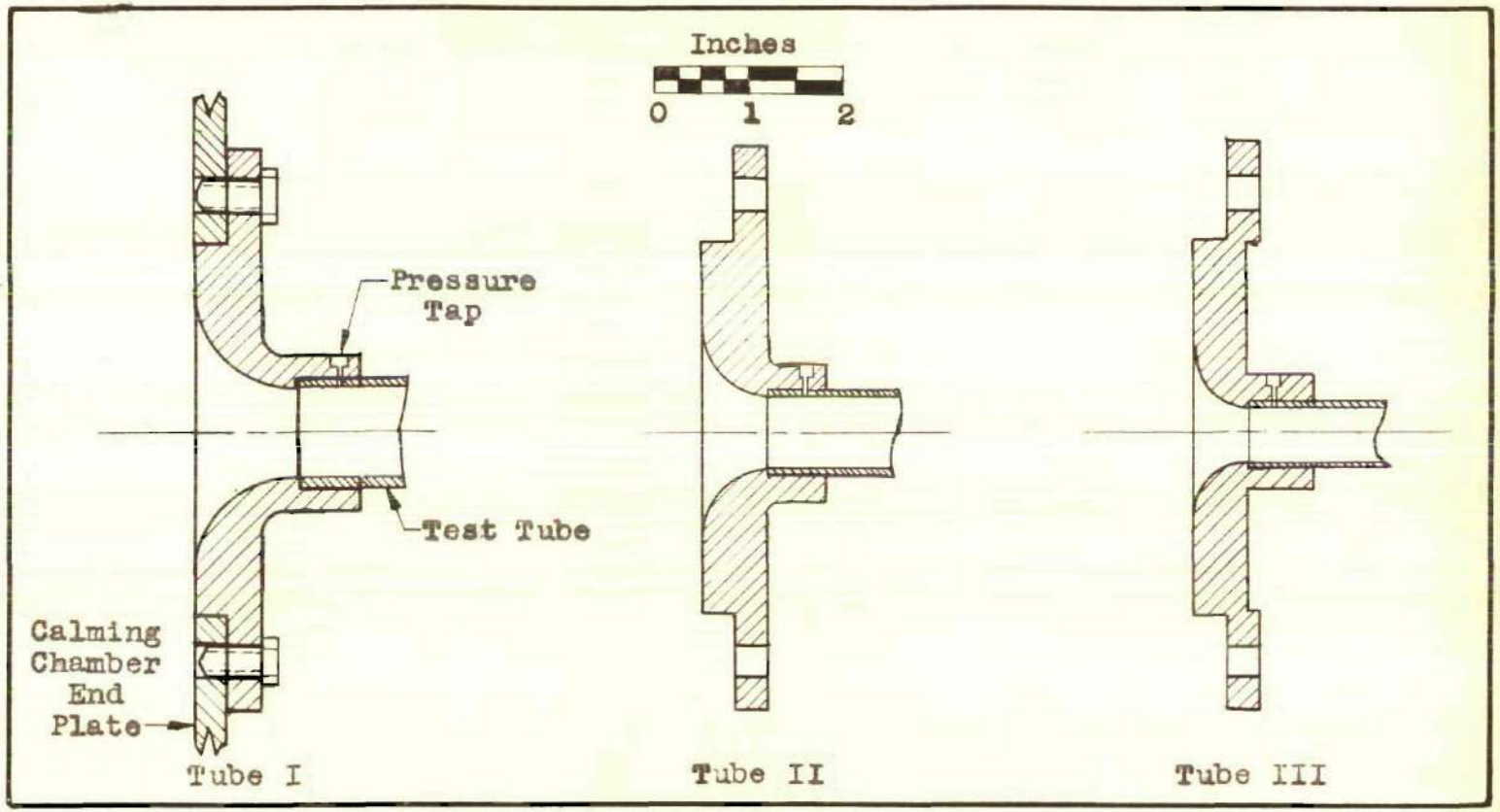

Figure 27. Details of Entry Sections

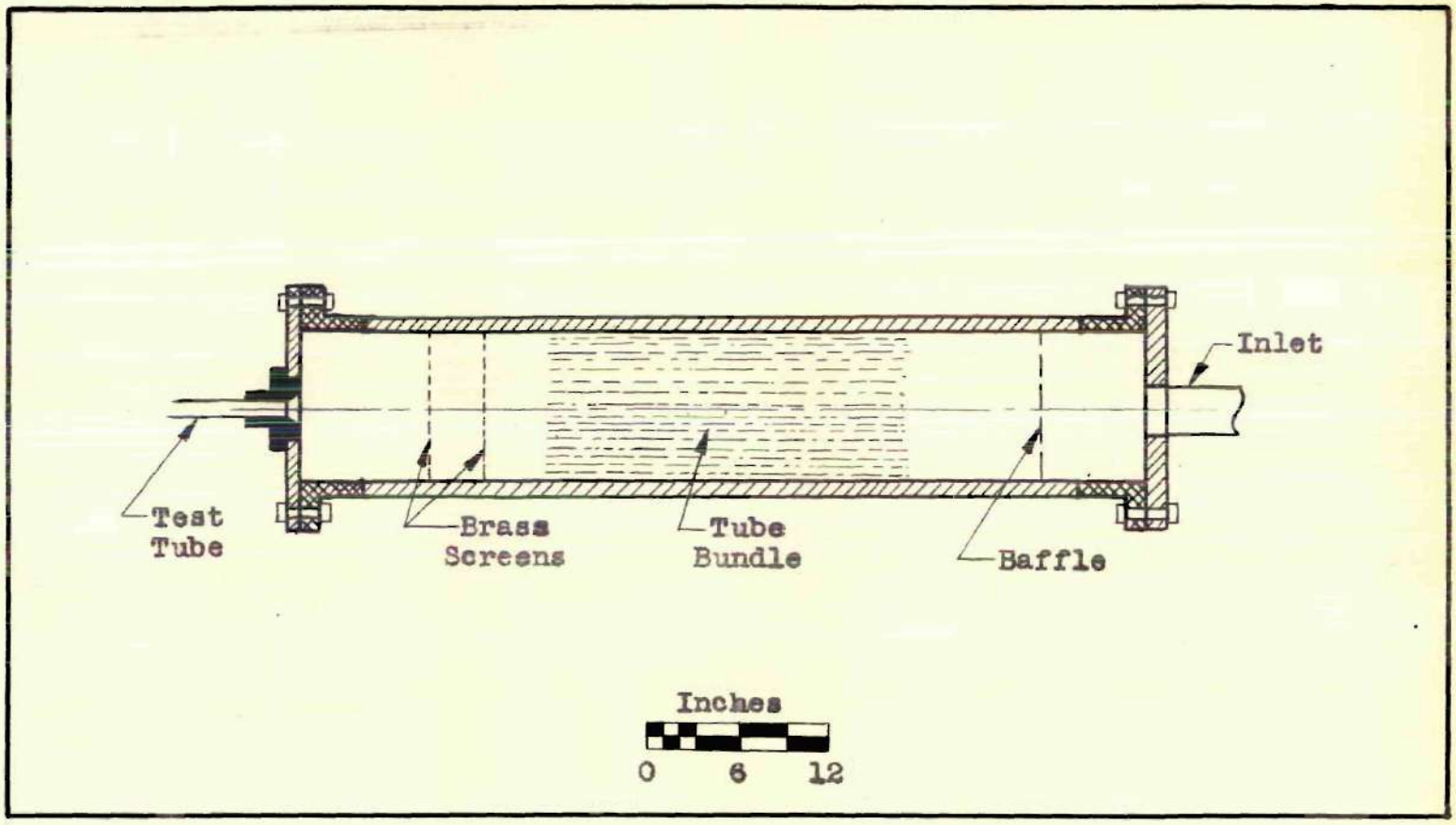

Figure 28. Details of Calming Chamber

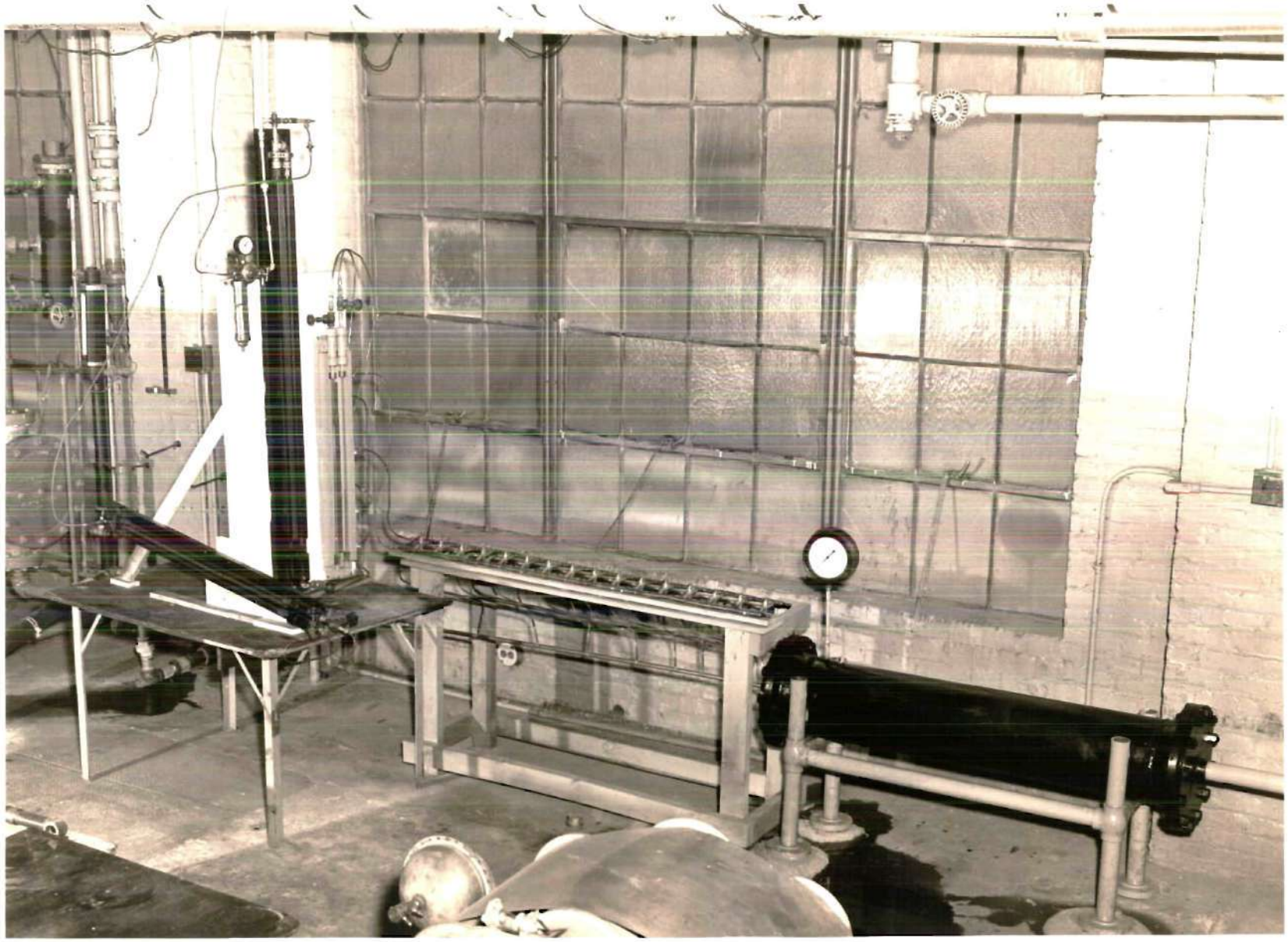

Figure 29

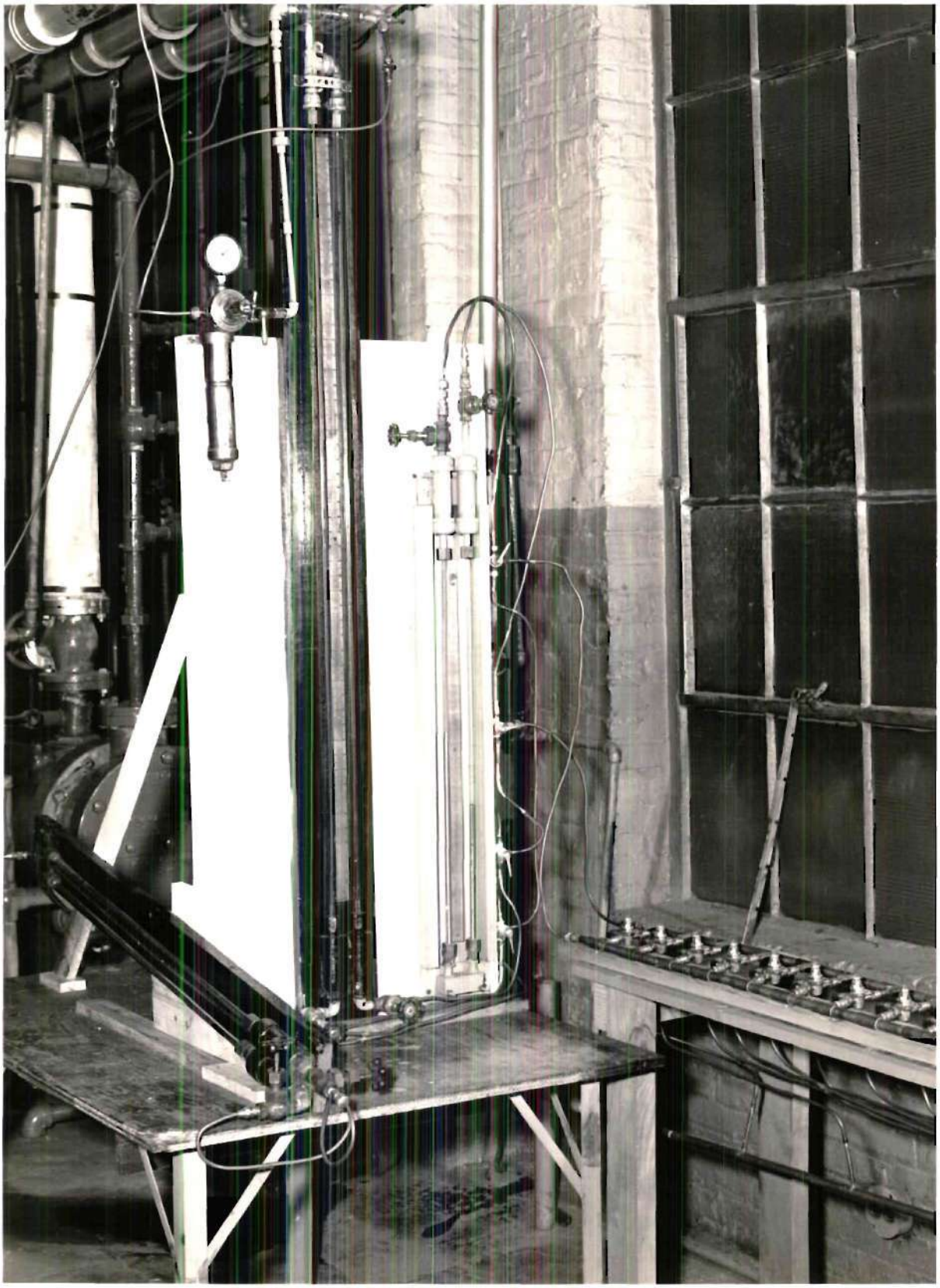

Figure 30

BIBLIOGRAPHY

1. Shapiro, A. H., and Smith, R. D., Friction Coefficients in the Inlet Length of Smooth Round Tubes, N.A.C.A. Technical Note #1785, Nov. 1948, p. 3.

2. Loc. cit.

3. Langhaar, H. L., "Steady Flow in the Transition Length of a Straight Tube," Journal of Applied Mechanics, vol. 9, June 1942, pp. 55-58.

4. Shapiro and Smith, op. cit., p. 4.

5. Loc. cit.

6. Egli, A., "The Leakage of Gases Through Narrow Channels," Journal of Applied Mechanics, vol. 4, March 1937, p. 63.

7. Keenan, J. H., and Neuman, E. P., "Measurement of Friction in a Pipe for Subsonic and Supersonic Flow of Air," Journal of Applied Mechanics, vol. 13, June 1946, pp. 91-100.

8. Shapiro and Smith, op. cit.